DEFENCE RESEARCH ESTABLISHMENT
CENTRE DE RECHERCHES POUR LA DÉFENSE
VALCARTIER, QUÉBEC

DREV-TM-1999-050
Unlimited Distribution / Distribution illimitée

AERODYNAMIC COEFFICIENTS MEASUREMENT ON A MODEL OF A SPARROW AIM-7M MISSILE IN THE DREV TRISONIC WIND TUNNEL

by

É. Y. Fournier

July/juillet 1999

Approved by / approuvé par

Head, Delivery Systems Section
Chef, Section systèmes de lancement

21 July 99
Date

WARNING NOTICE

The information contained herein is proprietary to Her Majesty and is provided to the recipient on the understanding that it will be used for information and evaluation purposes only. Any commercial use, including use for manufacture, is prohibited. Release to third parties of this publication or of information contained herein is prohibited without the prior written consent of DND Canada.

© Her Majesty the Queen in Right of Canada as represented by the Minister of National Defence, 1999

ABSTRACT

The present wind tunnel investigation is part of a project studying the effectiveness of reaction jet controls on missiles and projectiles. As a comparison basis between reaction jets and conventional control appendages was required, a complete database of aerodynamic coefficients had to be developed on a generic model shape. However, instead of using a generic model, it was decided to use a model of the Sparrow AIM-7M medium range missile in an effort to demonstrate the capability of DREV's wind tunnel in the experimental investigation of actual missiles, and also due to the large aerodynamic database existing on this vehicle. Testing covered a large range of Mach numbers, from 1.5 to 4.0, and angles of incidence from -10° to + 10°. Two different roll orientations of the model were studied (0° and 45°). Additionally, data involving wing deflections were also generated for the same Mach number range, over the same model incidence range, for deflection angles up to 20°. A build-up component method was used during the testing phase: data for a clean body (F1), for a body with tail fins only (F3), for a body with control wings only (F2), for a body with both sets of appendages (F4), and finally, for a body with both sets of appendages and antennas and attachment pins (F5) were generated. The database for the reaction jet project was generated and comparative results have indicated that DREV's wind tunnel can generate good technical results for missile shaped models.

RÉSUMÉ

La présente série d'essais en soufflerie fait partie d'un projet portant sur l'étude de l'efficacité des jets latéraux pour le contrôle de projectiles et de missiles. Comme le besoin d'une base de comparaison entre les jets latéraux et les méthodes de contrôle conventionnelles était évident, on a décidé de constituer une banque de données sur les coefficients aérodynamiques pour un modèle de missile générique. Cependant, au lieu d'un missile générique, on a choisi d'utiliser un modèle du missile à moyenne portée Sparrow AIM-7M, en raison de la grande quantité d'information aérodynamique existant sur ce missile. De plus, l'utilisation d'un missile avec des coefficients aérodynamiques connus a permis de démontrer la capacité de la soufflerie trisonique du CRDV d'étudier ce type de corps à long allongement et avec de grandes surfaces de contrôle. Les essais ont été effectués pour une plage de nombre de Mach de 1,5 à 4,0, et pour des angles d'incidence de -10° à + 10°. En plus, nous avons étudié le modèle à deux angles de roulis (0° et 45°). Finalement, on a colligé des données pour des angles de déflexion des surfaces de contrôle jusqu'à 20°, pour les mêmes plages de nombres de Mach et d'angles d'incidence du missile. On s'est servi pour ces essais d'une méthode d'addition des composantes: on a généré des données pour un corps seul (F1), pour un corps avec des ailettes arrière seulement (F3), pour un corps avec des ailes de contrôle seulement (F2), pour un corps avec les ailettes et les ailes de contrôle (F4), et finalement, pour un corps avec les ailettes, les ailes de contrôle ainsi que les antennes et les supports d'attache. On a constitué une base de données pour le projet des jets latéraux, et les résultats comparatifs ont démontré que la soufflerie trisonique du CRDV permet d'obtenir de bons résultats techniques pour des modèles de cette forme.

TABLE OF CONTENTS

ABSTRACT / RÉSUMÉ i

TABLE OF CONTENTS iii

EXECUTIVE SUMMARY v

NOMENCLATURE vii

1.0 INTRODUCTION 1

2.0 EXPERIMENTAL SITE AND INSTRUMENTATION 1

3.0 MODELS AND TEST CONDITIONS 3

4.0 RESULTS AND COMPARISONS 6

4.1 Balance Overload Test 6
4.2 Testing Results 8
4.3 Testing Sequence Modifications Due to Balance Problems 12
4.4 Testing With Overload Balance 13

5.0 CONCLUSIONS AND RECOMMENDATIONS 18

6.0 ACKNOWLEDGEMENTS 18

7.0 REFERENCES 19

TABLES I to III

FIGURES 1 to 17

APPENDIX A - Testing Schedule

APPENDIX B - Selected Model Drawings

APPENDIX C - Tabulated Results

APPENDIX D - Results

EXECUTIVE SUMMARY

Air-to-air missiles have been part of the Canadian Forces inventory for several decades. At present, the Sidewinder AIM-9 short-range IR missile and the Sparrow AIM-7M medium range missile are the two major components of the Air Force inventory. These missiles use traditional aerodynamic appendages to provide control during their flight. The introduction of reaction/lateral jet control systems in the missile industry is currently modifying the role of control appendages as development programs are under way around the world (US, UK, France, and others) to study and use the potential of RJC systems. Reaction jet flight control systems can provide extended improvements in terms of manoeuvrability, response time, and drag. However, a thorough understanding of the complex aerodynamic effects induced by the injection of transverse jets into a supersonic freestream is required before using this new technology in a design phase.

In order to develop a knowledge base and an expertise with this new technology in the field of control systems, the Defence Research Establishment Valcartier (DREV) has been involved in a research project to study the aerodynamic performance of vehicles guided by reaction jet controls. The specific objective of this study is to improve our understanding of the possible threat posed from weapons using these systems and to exploit this new technology in our own development efforts. The overall research project involves numerical studies, wind tunnel investigations and free-flight firings of various configurations of vehicles. The current phase of the project involved the development of an aerodynamic coefficient database about a generic missile with appendages, to serve as a baseline performance comparison with this new control technology. However, in order to evaluate the capacity of the DREV wind tunnel in generating accurate results for missile testing, an actual missile, the Sparrow AIM-7M, was selected as a baseline.

This investigation is composed of a wind tunnel experiment to measure forces and moments on a scaled-down model (approximately 15% of the original dimensions) of the Sparrow AIM-7M air-to-air missile. The experiments were carried out for nominal Mach numbers of 1.5, 2.0, 2.5, 3.0, 3.5 and 4.0. Several roll positions, fin orientations (up to 20°) and missile pitch angles were also investigated.

With the use of several configurations, a complete aerodynamic coefficient database was generated for the model, over the range of Mach numbers from 1.5 to 4.0, and for angles of incidence from -10° to + 10°. Additionally, data involving wing deflections were also generated for the same Mach number range, over the same model incidence range, for deflection angles up to 20°. Thus, a fairly comprehensive database was generated by this experiment. Comparisons with actual AIM-7F data have shown that DREV's Trisonic Wind Tunnel can provide results comparing well with actual missile bodies. Thus, high l/d bodies with large appendages can successfully be tested in this facility.

VI

NOMENCLATURE

A	Axial force
a	Distance between balance reference center and N_1 plane of reference
b	Distance between balance reference center and N_2 plane of reference
C_M	Pitching moment coefficient
C_N	Normal force coefficient
d	Model reference diameter
e	Distance between balance reference center and S_1 plane of reference
f	Distance between balance reference center and S_2 plane of reference
N_1	Forward normal force with respect to balance reference system
N_2	Aft normal force with respect to balance reference system
Q	Wind tunnel dynamic pressure
Roll	Rolling moment (measured by balance)
S	Model reference cross-sectional area
S_1	Forward side force with respect to balance reference system
S_2	Aft side force with respect to balance reference system
X_{CP}	Center of pressure
α	Model angle of incidence to the flow

1.0 INTRODUCTION

Air-to-air missiles have been part of the Canadian Forces inventory for several decades. At present, the Sidewinder AIM-9 short-range IR missile and the Sparrow AIM-7M medium range missile are the two major components of the Air Force inventory. These missiles use traditional aerodynamic appendages to provide control during their flight. The introduction of reaction/lateral jet control (RJC) systems in the missile industry is currently modifying the role of control appendages as development programs are under way around the world (US, UK, France, and others) to study and use the potential of RJC systems. The current wind tunnel investigation is part of a project studying the effectiveness of reaction jet controls on missiles and projectiles (Ref. 1). As a known base missile configuration was required to allow for performance comparisons, it was decided to use the Sparrow AIM-7M, which has been in service with the Canadian Air Force for several years, and on which experimental aerodynamics data exists. Another important objective behind the use of a known missile is the validation of the DREV wind tunnel for missile aerodynamic studies. High length-to-diameter ratio (l/d) projectiles have previously been tested in this wind tunnel facility, but the use of a high l/d body, with large and multiple control surfaces is a first for this facility. The success of the missile validation for DREV's wind tunnel would certainly lead to an increase use of this facility for this type of experimental work.

This investigation is composed of a wind tunnel experiment to measure forces and boundary layer characteristics on a scaled-down model (approximately 15% of the original dimensions) of the Sparrow AIM-7M air-to-air missile. The results from the boundary layer characteristic study have been reported in a separate report (Ref. 2). The experiments were carried out for nominal Mach numbers of 1.5, 2.0, 2.5, 3.0, 3.5 and 4.0. Data for a Mach number of 3.5 were used more extensively for validation purposes, as a change of wind tunnel balance forced us to run several additional tests to verify the accuracy of the results (more details in Sections 4.2 and 4.3). Several roll positions, wing orientations (up to 20°) and missile pitch angles were also investigated.

This work was conducted at Defence Research Establishment Valcartier (DREV) between October 1996 and May 1998, under Project 3EB12 - Flight Dynamics for Missile Performance Studies.

2.0 EXPERIMENTAL SITE AND INSTRUMENTATION

The DREV wind tunnel, shown schematically in Fig. 1, is an intermittent, in-draft wind tunnel with a 0.6m x 0.6m test section. Because of its in-draft characteristic (air flowing from an atmospheric pressure tank to a vacuum tank), values of Reynolds numbers are lower than the free-flight values during tests at high Mach numbers. The range of Reynolds numbers for this test series varied between 15.2×10^6 /m (for Mach number = 1.5) to 6.0×10^6 /m (for Mach number = 3.5). Tests were performed at 6 Mach numbers (1.5, 2.0, 2.5, 3.0, 3.5 and 4.0). The useful duration of testing for these conditions was around 7 seconds.

Two types of testing were performed with this model. Initially, boundary layer surveys were conducted at several locations on the model surface to determine the thickness of the boundary layer at these locations. These results have been presented in a separate report (Ref. 2). In the second part of the testing sequence, a series of force and moment measurements were performed using wind tunnel balances. For these tests, the model was swept (in pitch) over a range of angles of attack varying between -10° and +10° for the six Mach numbers under investigation. The model was also tested at different roll indexation angles (0°, 45°, 90°, 135°, and 180°) (see Appendix A for a list of runs). Simultaneously, the base pressure was measured (Kulite SVQH-500-10 pressure transducer) to allow the data analysis system to calculate the base drag and provide the forebody drag component of the total drag. Thereafter, aerodynamic coefficients were derived from the test results.

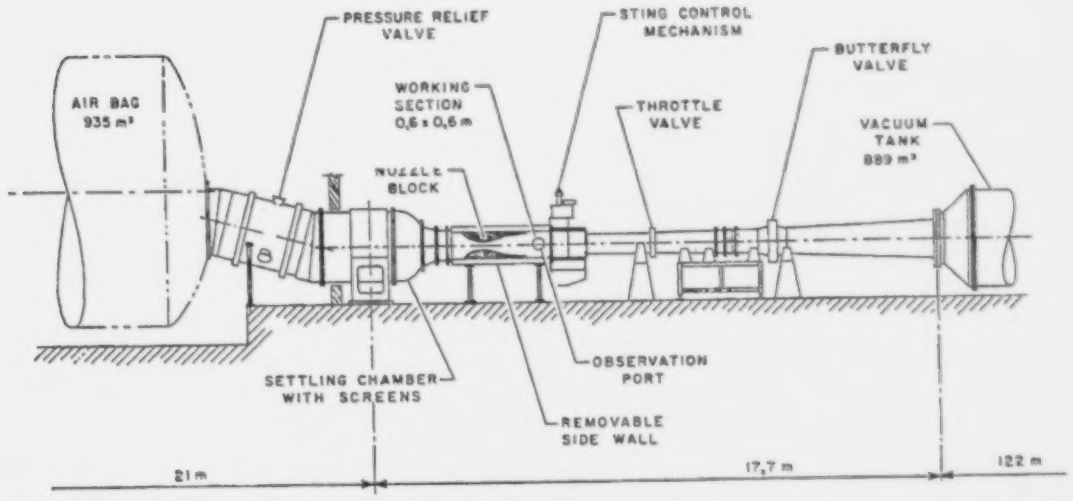

FIGURE 1 – DREV intermittent in-draft wind tunnel

Two wind tunnel balances were used for these tests. Prior to the actual series of wind tunnel tests, a 0.75 inch five degrees of freedom overload balance was used to determine the maximum loads experienced by the model in the wind tunnel under the various testing conditions. This balance has no axial force element. It was designed by the University of Sherbrooke, under a DREV contract in 1988 (Ref. 3). During the actual series of tests, a six degrees of freedom 0.75 inch ABLE MK-XIX-C balance was used to produce highly accurate results.

Standard instrumentation (Pitot tubes, wall pressure taps and temperature probes) located in the plenum chamber and in the test section were used to monitor the tunnel free stream conditions. Static pressures were measured by means of Rosemount pressure transducers. After each run, analog results from the balance and other data acquisition instrumentation (including the results from the tare run) were digitized and stored for further transformation through the data reduction software.

The major equations used to reduce the raw data into useful aerodynamic coefficients are presented in Table I.

TABLE I

Aerodynamic Coefficient Equations

CA (axial force coefficient)	= A / QS
CN (normal force coefficient)	= $(N_1 + N_2)$ / QS
CL (lift coefficient)	= (CN cos α) – (CA sin α)
CDT (total drag coefficient)	= (CA cos α) +(CN sin α)
CRM (rolling moment coefficient)	= roll / (QSd)
CM (pitching moment coefficient)	= $\{(N_1 a) – (N_2 b)\}$ / QSd
CY (side force coefficient)	= $(S_1 + S_2)$ / QS
CYM (yawing moment coefficient)	= $\{(S_1 e) – (S_2 f)\}$ / QSd
XCP (center of pressure)	= - (CM / CN)

As part of the data reduction process, several of the coefficients introduced in Table I are plotted against model angle of incidence. The slope of these curves for several of the coefficients are then calculated (slope values between -5° and +5° of model incidence). Two of these results (normal force coefficient slope and pitching moment coefficient slope) have been used extensively in the analysis phase of this experiment.

3.0 MODELS AND TEST CONDITIONS

The missile to be tested is shown in Fig. 2, along with its sting supporting system. A photograph of the model mounted in the wind tunnel is also shown in Fig. 3. It is a 1 to 7 ratio model of the Sparrow AIM-7M air-to-air missile. This model has an ogival nose and a 30 mm diameter cylindrical main body, for a total model length of 531 mm. The l/d of the model is 17.7. The sting to model diameter ratio for this model is 0.677, and the sting length aft of the body is less than 1 caliber. Thus, the presence of this large sting will disturb the flow around the base, causing an error in the base drag component.

This model has been designed and built in 3 modules, to allow for parametric aerodynamic studies of different body configurations. The first module is for the nose of the model, and has a length of 6.24 calibers. The second module is for the mid-section of the missile, and it has a length of 4.43 calibers. This module is used to house the wind tunnel balance during force measurements, and is the section which will be modified in subsequent testing to also house the lateral reaction jet generating system. Three different second modules have been built: one without wings installation set-up (clean body), one with wings installation set-up allowing for odd angles of attack (10°, 30°), and the last one with wings installation set-up allowing for even angles of attack (0°, 20°). Finally, the third module is the tail section of the body and is 7.03 calibers long. Two versions of this module have been designed and built. The first one is a module with the fixed fins of the

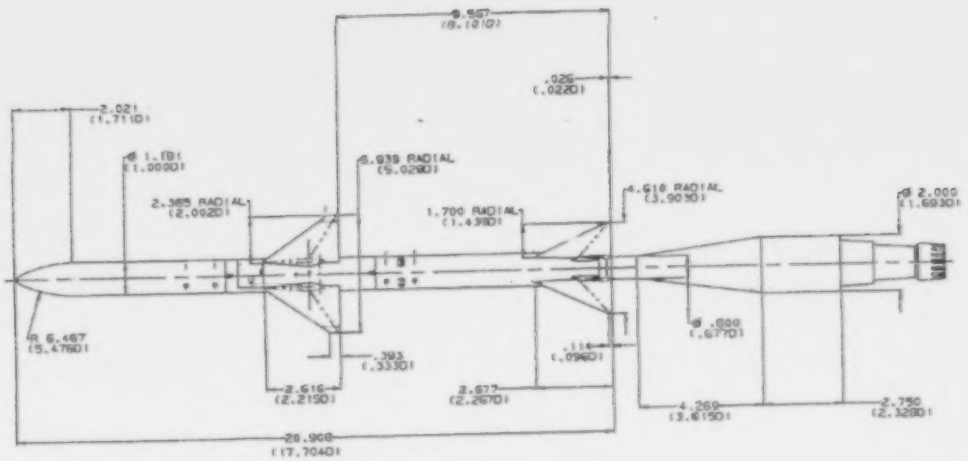

FIGURE 2 - Schematic of the model (dimensions in inches, with non-dimensional values relative to the model diameter in brackets)

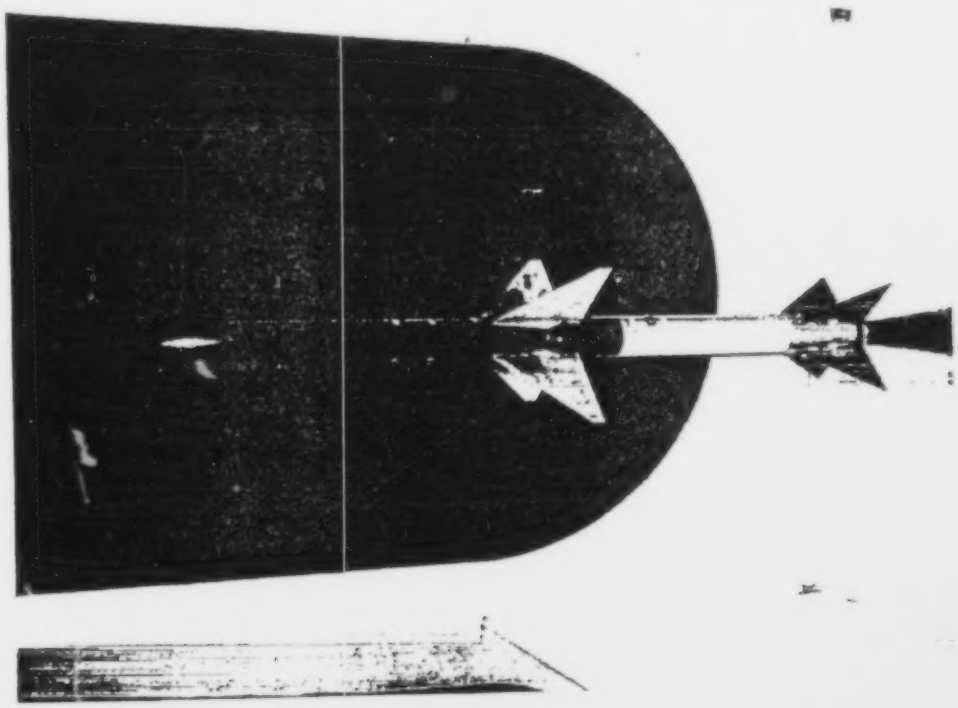

FIGURE 3 - Photograph of the model

Sparrow missile, while the second one is again a body without any fins (clean body). Finally, removable antennas and attachment pins have also been designed. Thus, 5 configurations have been designed and have been tested: a completely clean body (F1), a body with fins only (F3), a body with control wings only (F2), a body with both sets of appendages (F4), and finally, a body with both sets of appendages and antennas and attachment pins (F5). These configurations will allow for the development of a substantial database about the AIM-7M Sparrow missile, and permit comparisons with experimental results. Two specific missile roll orientations have been selected for performing wind tunnel parametric studies: 0° and 45° (+ and X configurations respectively). Table II shows each one of these 5 configurations. Appendix B shows drawings of various selected model components. Some of the results (for example, the pitching moment coefficient) have been referenced to the relative position of the center of gravity on the real AIM-7M Sparrow missile (9.125 body diameter from the missile nose).

TABLE II

Model configurations

Configuration F1

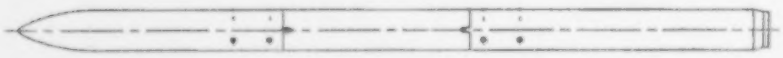

Configuration F2

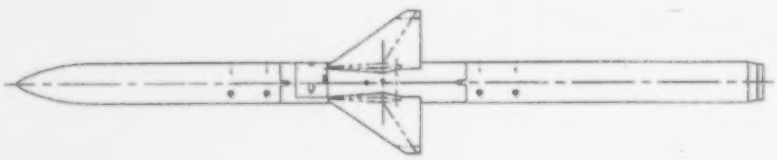

Configuration F3

Configuration F4

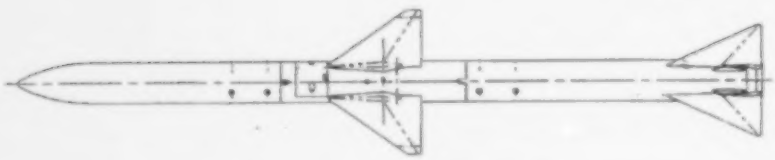

Configuration F5

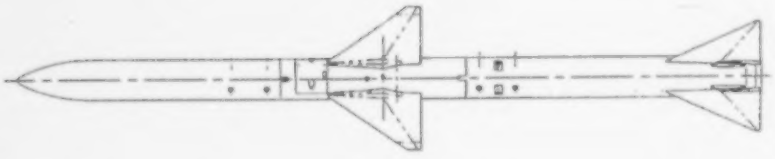

4.0 RESULTS AND COMPARISONS

4.1 Balance Overload Tests

Prior to testing with the high accuracy ABLE balance, a more robust (but less accurate for small loads) balance was used to study the overall forces and moments on the model during the testing sequence. High loads can be generated during three phases of a test in the DREV wind tunnel: at valve opening, at valve closing and for maximum angle of attack loads. Thus, specific model and testing configurations presenting the largest potential for dangerous loads were selected for evaluation during this sequence. A total of 21 runs were performed with the overload balance. A complete listing of these runs is provided in Table III.

TABLE III

Overload test sequence

Test Number	Run Number	Configuration	Sweep Angles	Model Roll Angle	Fin Angle	Mach Number
F2.20.+.00.1.sur	R6323	Body + control wings	-10° to +10°	+	0°	2.0
F2.20.+.00.2.sur	R6325	Body + control wings	-10° to +10°	+	0°	2.0
F2.20.+.20.1.sur	R6326	Body + control wings	-10° to +10°	+	20°	2.0
F4.20.+.00.1.sur	R6327	Body + control wings + fins	-10° to +10°	+	0°	2.0
F4.20.+.00.2.sur	R6328	Body + control wings + fins	-10° to +10°	+	0°	2.0
F4.20.+.20.1.sur	R6329	Body + control wings + fins	-10° to +10°	+	20°	2.0
F4.20.x.20.1.sur	R6330	Body + control wings + fins	-10° to +10°	x	20°	2.0
F2.25.+.00.1.sur	R6335	Body + control wings	-10° to +10°	+	0°	2.5
F2.25.+.00.2.sur	R6336	Body + control wings	-10° to +10°	+	0°	2.5
F2.25.+.20.1.sur	R6337	Body + control wings	-10° to +10°	+	20°	2.5
F4.25.+.00.1.sur	R6333	Body + control wings + fins	-10° to +10°	+	0°	2.5
F4.25.+.00.2.sur	R6334	Body + control wings + fins	-10° to +10°	+	0°	2.5
F4.25.+.20.1.sur	R6332	Body + control wings + fins	-10° to +10°	+	20°	2.5
F4.25.x.20.1.sur	R6331	Body + control wings + fins	-10° to +10°	x	20°	2.5
F2.35.+.00.1.sur	R6339	Body + control wings	-10° to +10°	+	0°	3.5
F2.35.+.00.2.sur	R6340	Body + control wings	-10° to +10°	+	0°	3.5
F2.35.+.20.1.sur	R6338	Body + control wings	-10° to +10°	+	20°	3.5
F4.35.+.00.1.sur	R6341	Body + control wings + fins	-10° to +10°	+	0°	3.5
F4.35.+.00.2.sur	R6342	Body + control wings + fins	-10° to +10°	+	0°	3.5
F4.35.+.20.1.sur	R6343	Body + control wings + fins	-10° to +10°	+	20°	3.5
F4.35.x.20.1.sur	R6344	Body + control wings + fins	-10° to +10°	x	20°	3.5

These tests were mainly selected because of high dynamic pressure and/or configurations with appendages. As the objective was to identify maximum loads, no filtering was applied on the data from the data acquisition system. Additionally, this system was collecting at a high frequency rate, to allow for the identification of possible

short loading peaks. However, as these data are still discrete data, there still exists a chance for a larger load to affect the model and not be recorded by the data acquisition system.

Figure 4 shows 4 graphs of results from the overload test sequence. The first two (a and b) show results for the F2 configuration (run R6323, first run of the series), while the next two (c and d) show the same results for the F4 configuration (run R6327, fifth run of the series). A change in the testing procedure was initiated from these preliminary results.

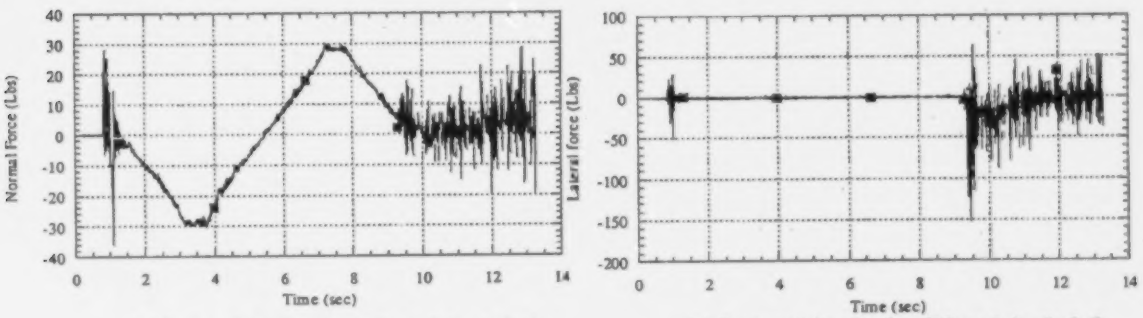

a) Normal force for F2 at Mach 2.0

b) Lateral force for F2 at Mach 2.0

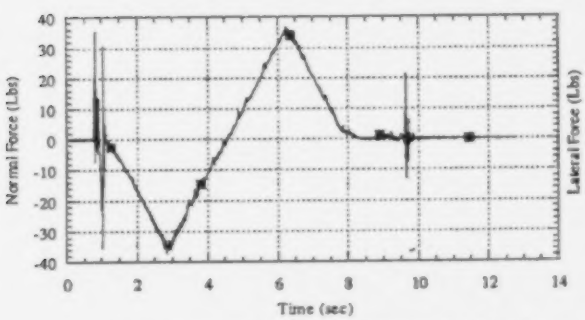

c) Normal force for F4 at Mach 2.0

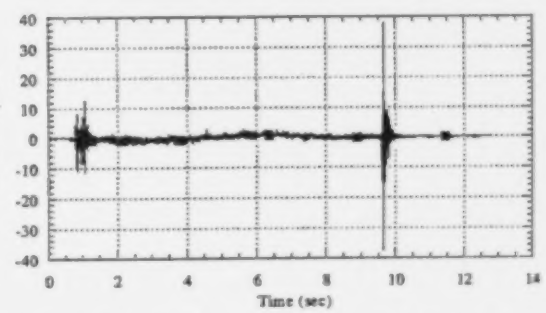

d) Lateral force for F4 at Mach 2.0

FIGURE 4 – Overload test results

In Figs. 4 a) and b), the closing of the wind tunnel valve occurs 13.5 seconds after the beginning of the experiment. This long testing time leads to the balance being subjected to large force variations as the flow becomes unstable in the tunnel (decreasing pressure ratio between vacuum tank and air reservoir) in the last 4 seconds. A decision was made to accelerate the model sweeping speed to decrease the overall testing time (model back to wind tunnel centerline at 8.0 seconds, and closing at 9.5 seconds), and thus be able to shut the valve before the appearance of unsteady effects in the flow. Figures 4 c) and d) show the results from the first test using this new testing sequence. The effects on the balance at closure are reduced substantially. This new time sequence was adopted for the remaining of the experiment (including tests with the ABLE balance).

The technique used to analyze the results for possible balance overloads, either in forces or moments, for both lateral and normal directions is shown in Fig. 5. First, the ABLE balance maximum loads are displayed on the graph (Ref. 3). The large parallelepiped represents the normal plane capacity of the balance, while the small one represents the lateral plane capacity of the balance. Moments are displayed on the abscissa, while forces are displayed along the ordinate. Then, peak force and moment values are taken from results as the one shown in Fig. 4 for each configuration of interest. The normal force and pitching moment are then use to generate the normal plane maximum loading (empty squares) and compare with the maximum allowable (the large parallelepiped). For the present case, no problem exists with this plane. The same process is followed for the lateral plane (circles), and the results compared to the small parallelepiped. The results for the lateral loading are substantially closer to the maximum loading taken by the balance. In order to allow the use of the ABLE balance, the two loading lines had to stay inside their respective parallelepiped. Thus, the present case (Fig. 5) and others of its type would be assumed not to present any danger to the ABLE balance. However, several cases, mostly for higher dynamic pressures (Mach 2.0 and 2.5) had to be removed from the testing list in order not to damage the ABLE balance.

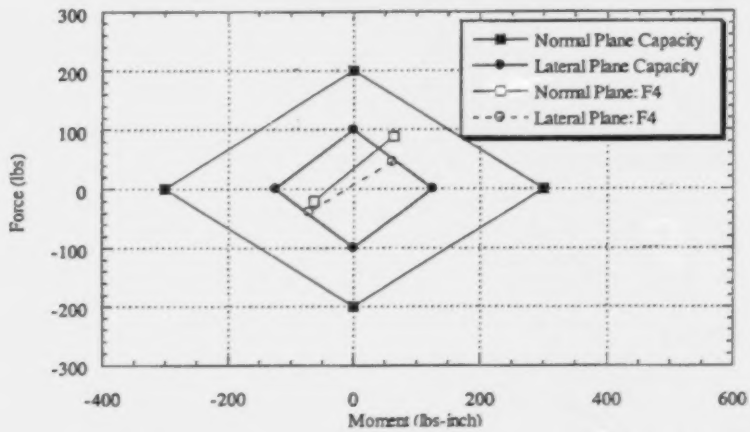

FIGURE 5 – Balance capacity comparisons : F4 at Mach 3.5

4.2 Testing Results

As the model was built in 3 separate modules, it was necessary to verify the concentricity of the modules to the centerline of the model and sting assembly. Thus, the first few tests were carried out at Mach 2.0 and 2.5 on the clean model (no fins) to verify this geometric parameter. Through a series of tests involving pitching the model from -10° to +10° for various roll indexation angles (0°, 45°, 90°, 135°, and 180°), it was discovered that a concentricity problem existed with the model. Figure 6 shows some of the axial force curves for the different roll angles. The curve at a roll indexation of 90° shows a result substantially different than the other curves. After examination, it was discovered that the nose module of the Sparrow model was built a few thousandths of an inch out of

concentricity. After re-machining the nose section, the same type of tests showed that the lack of concentricity had been largely eliminated.

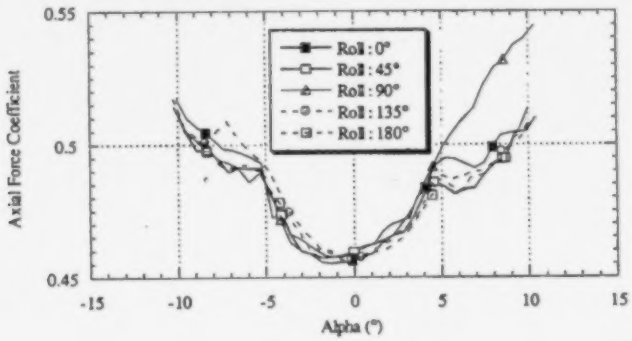

FIGURE 6 – Axial force coefficient for clean body at Mach 2.0

The remaining phase of this testing sequence was divided in 6 sections, one for each one of the Mach numbers. The first Mach number to be tested was Mach 3.5, and the tests followed the configuration numbers F1 to F5, in a chronological order, so as to build on the model as the testing progressed. These tests were performed for a 0° angle of attack of the wings of the missile. They were then followed by the tests for angles of attack on the wings, for all missile configurations (F2, F4 and F5). All these tests were performed for two roll orientations: 0° and 45° (+ and X configurations respectively). The same testing method was then used for the other Mach numbers to be tested.

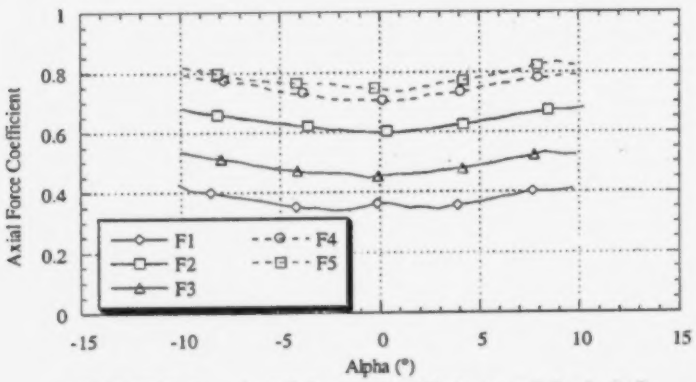

FIGURE 7 – Axial force coefficient at Mach 3.5

As the amount of data generated by this wind tunnel series is substantial, only some specific results will be demonstrated is this report. A listing of all test cases can be found in Appendix A.

Figure 7 shows the axial force coefficient for all 5 configurations tested at Mach 3.5 (wings at 0°). The relative increase in drag produced by the various missile components (wings (F2), fins (F3), and attachments (F5)) can easily be determined from

this figure. One interesting result is the large drag increase generated by the antennas and the support system of the missile (around 6%), which certainly leads to a decrease in the actual maximum range of this weapon.

Data for the F4 configuration will now be used to support the main objective of this experiment which was to present the potential of this facility in providing accurate results for missile models. Reference 5 provided wind tunnel results for the Sparrow AIM-7F missile. The only major geometric difference between the 7F and the 7M version is a modification to the nose shape of the 7M model, which should lead to an increase in drag. This increase in drag has been calculated (numerical simulation with a semi-empirical code, AP-81 (Ref. 4)) to be around 10%. No effect on the normal force and the pitching moment are expected.

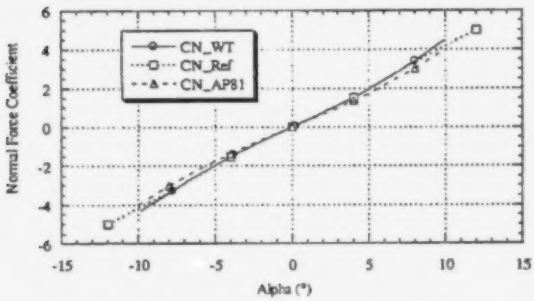

a) Normal force coefficient

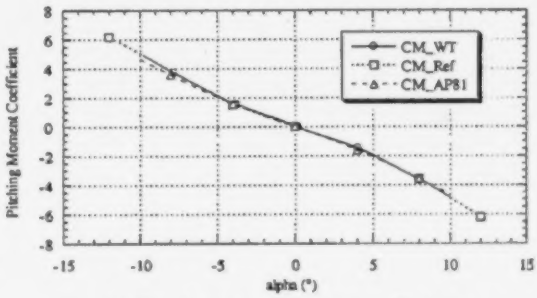

b) Pitching moment coefficient

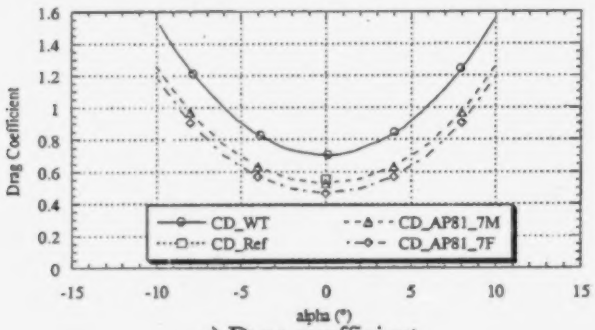

c) Drag coefficient

FIGURE 8 – Results for the F4 configuration (+) at Mach 3.5

Figure 8 shows results for the F4 model, for a "+" configuration. The axial force, the normal force and the pitching moment coefficients are shown again at Mach 3.5, between 10° to +10°, and are compared to actual wind tunnel Sparrow AIM-7F data (Ref. 5) and data generated by the semi-empirical code mentioned previously. Figure 9 shows the same type of results, but for a "X" configuration.

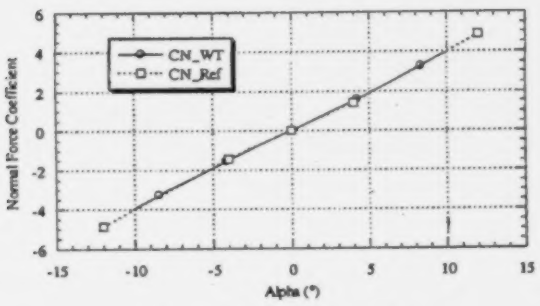

a) Normal force coefficient

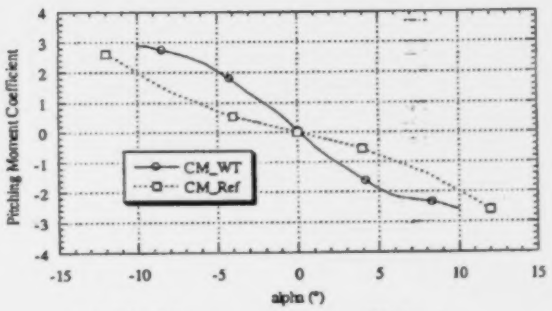

b) Pitching moment coefficient

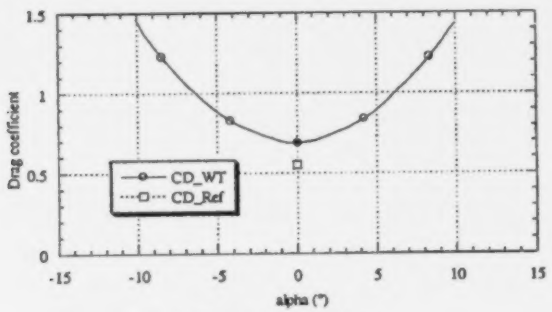

c) Drag coefficient

FIGURE 9 - Results for the F4 configuration (X) at Mach 3.5

The agreement between the 3 sources of data for the normal force and the pitching moment coefficients is good. The results from AP-81 tend to deviate from the two other curves for larger angles of incidence (above 7°), but it is a known weakness of this semi-empirical code. The results from the DREV wind tunnel are never more than 3% away from the other experimental curves. The third graph of Fig. 8 shows results that seem to present substantially less agreement. It is the drag coefficient curve. Two major reasons explain the difference between the present wind tunnel results, and the results from Ref. 5: the geometric difference between the two missiles studied and the sting interference existing in the DREV facility for these tests. Firstly, the model studied in wind tunnel is the 7M configuration, while the literature results are for the 7F configuration. As mentioned previously, a small geometric difference exists between the nose sections of these two configurations. In order to quantify the effect of this difference on the drag of the missile, a drag curve for the AIM-7F calculated with AP-81 has also been added to the graph. Although AP-81 is empirical in nature, it should allow for relative comparisons of drag of the two missile variants. Comparing these two curves shows the relative drag increase between the two configurations to be around 8-10 % (increase from 7F to 7M). Secondly, the effect of sting interference accounts for the remaining of the difference between the two sets of experimental data. It has been shown (Refs. 6, 7) that the effect of the sting is to lead to an increase in the total drag value, which is shown in Fig. 8. Defining accurately the drag increase is complex, but for the Mach number range of the experiment,

and for the specific sting to body diameter ratio, it is between 10% and 15%. The pressure probe at the base of the model is also affected by the large support sting, and provides erroneous base pressure readings to the data reduction systems. Thus, total drag coefficient were used in the results as the base pressure values could not be determined accurately, and therefore could not be used to reduce the total drag values to other useful variables, such as forebody drag.

For the "X" configuration, the results for the normal force coefficient agree well with the values from the reference. For the pitching moment, the results from the present experiment follow the general trends shown by the actual AIM-7F results. However, the actual values seem to differ by up to 20% for some angles of incidence of the missile (inversion of the results about a 45° angle plane of symmetry). Finally, for the reasons introduced earlier, the wind tunnel drag results are slightly different than from the reference.

4.3 Testing Sequence Modifications Due to Balance Problems

After completing the Mach 3.5 testing sequence for the 0° angle of incidence on the wings, the middle module of the missile was changed to allow angles of incidence testing to take place. However, only one test (test # R6365: wings at 10°) was performed as the balance was damaged during the second test. The normal element N2 suffered a catastrophic failure. Because of the heavy loads associated with the use of this model, none of the other 0.75 inch ABLE balances available at DREV could be used to replace the damaged one. A decision had to be made between canceling and reporting the remaining tests to be performed, or using an overload balance to complete the testing, which meant the lost of the axial force parameter. Reporting meant to delay this experiment to the middle of 1999, as the only available wind tunnel testing time was in more than 15 months, and this course of action was not favored. It was then decided to reproduce one of the previous tests (F4 configuration, with wings at 0° angle of incidence) with the overload balance and compare the normal force coefficient, and the pitching moment coefficient to the values obtained with the ABLE balance.

Figure 10 shows some of the results from this comparison. The two most important parameters, the normal force and the pitching moment, are shown. The reproducibility of the results between the two balances is very good. There does not seem to be a lost of the sensitivity of the results with the overload balance, compare to the more precise ABLE instrument. The same comparisons were performed for various Mach numbers, and for various configurations, and the same type of results was generated. Thus, it was decided to proceed with the testing with the Sherbrooke overload balance. Additional testing will have to be performed at a later date to generate the drag coefficient, as the Sherbrooke balance is a five element balance (no axial force).

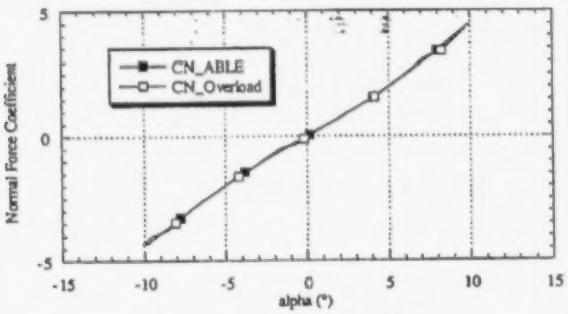

a) Normal force coefficient

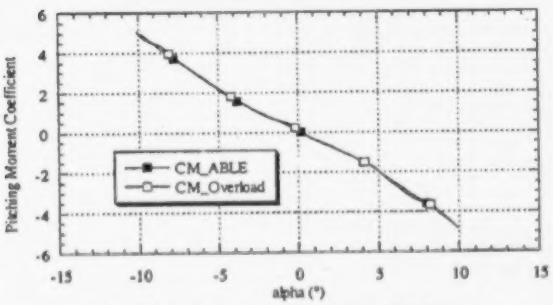

b) Pitching moment coefficient

FIGURE 10 – Comparison between two balances

4.4 Testing With Overload Balance

The testing schedule was thus followed as originally planned, with the exception that no drag coefficient could be compared with the results generated by the Sherbrooke balance. Additionally, it was decided to add some tests at two other Mach numbers: Mach 1.5 and 4.0.

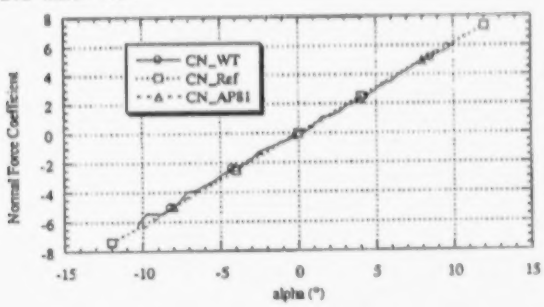

a) Normal force coefficient

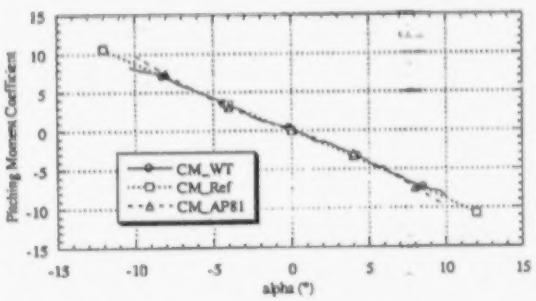

b) Pitching moment coefficient

FIGURE 11 - Results for the F4 configuration (0° roll) at Mach 2.0

Figure 11 shows results for the F4 configuration, at Mach 2.0 and for a 0° roll angle. As presented in Section 4.2, results from semi-empirical calculations with AP-81, and from the actual Sparrow data file have been added to these diagrams for comparison.

The normal force coefficient results (Fig. 11 a) demonstrate a very good agreement between the three sources of data. No significant differences are visible between these three curves. Figure 11 (b) shows the pitching moment coefficient results for the same configuration, and from the same three sources. Again, the agreement between these curves is very good. However, small variations begin to appear between the results at higher angles of attack (around 7°).

Large quantities of data were generated during this experiment. In order to reduce the number of graphs required to present a significant part of these results, with the goal of evaluating the wind tunnel with this type of model, the slope of the normal force coefficient (C_{NA}) and of the pitching moment coefficient (C_{MA}) are used. The next 2 figures (Figs. 12 and 13) show C_{NA} and C_{MA} for the 0° roll configuration, from Mach 1.5 to 4.0. These values are again compared to semi-empirical values (from AP-81) and to experimental values from the missile database.

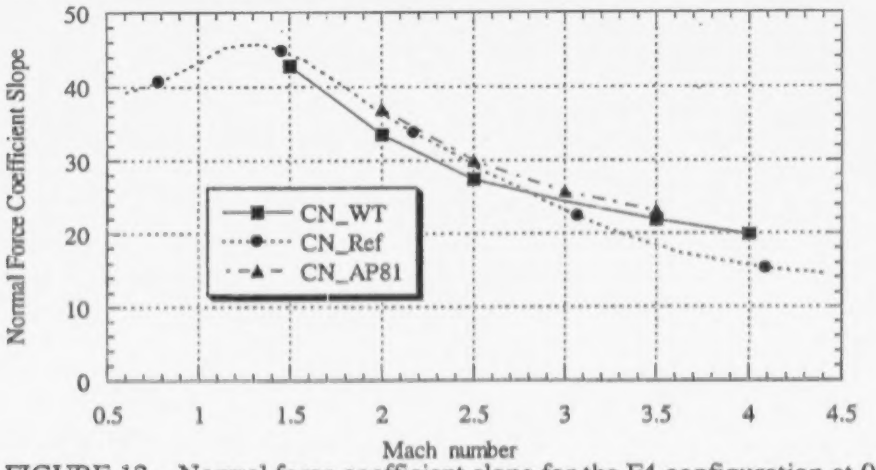

FIGURE 12 – Normal force coefficient slope for the F4 configuration at 0° roll

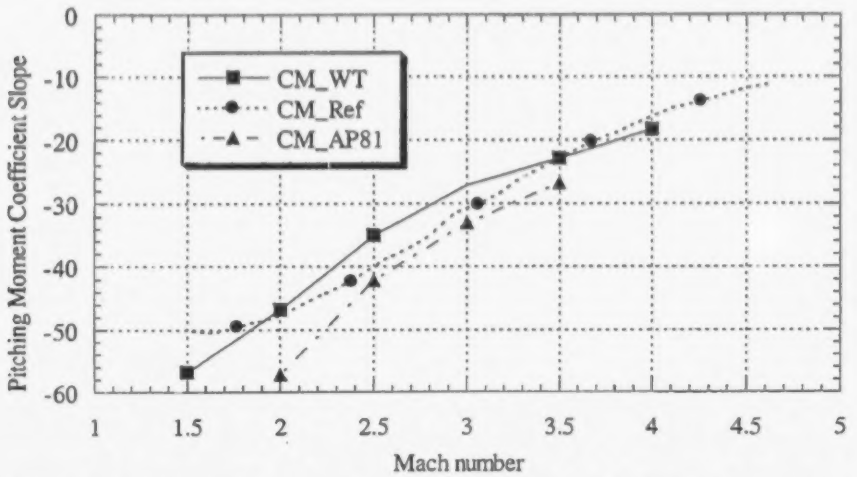

FIGURE 13 – Pitching moment coefficient slope for the F4 configuration at 0° roll

The following two figures (Figs. 14 and 15) show the same type of information, but for the 45° roll configuration. Because of the roll orientation of the model, it was not possible to generate AP-81 data for these cases.

The trends demonstrated by the actual missile data (curves from reference) were well followed by both the DREV wind tunnel data, and the AP-81 results, for the 0° roll orientation. On average, the difference between wind tunnel results (DREV) and actual values varied from 2% up to around 10%. The results from AP-81 presented relative errors larger than these values (up to around 20%).

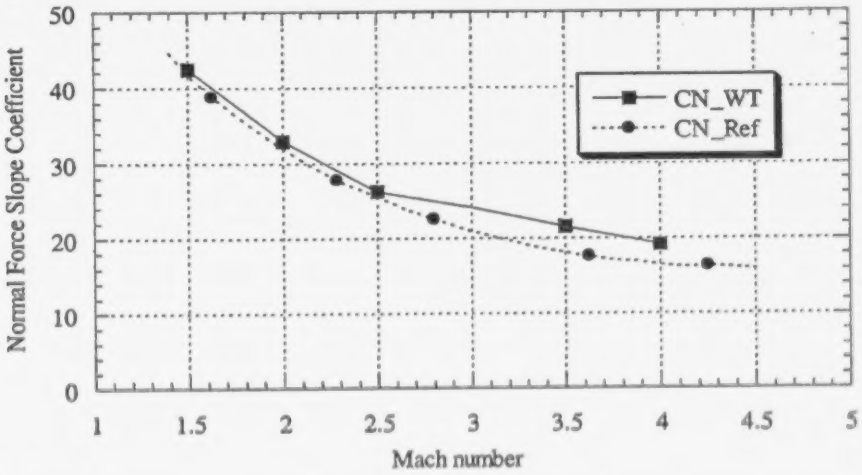

FIGURE 14 – Normal force coefficient slope for the F4 configuration at 45° roll

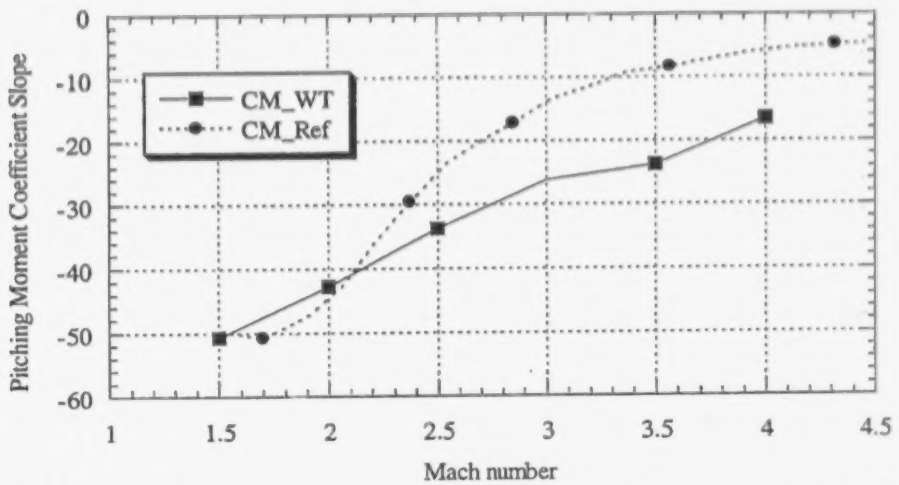

FIGURE 15 – Pitching moment coefficient slope for the F4 configuration at 45° roll

The results for the 45° roll orientation, at least for the pitching moment coefficient, are not as accurate as for the 0° roll orientation (Figs. 12 and 13). The results for the normal force coefficient are still fairly accurate, but more discrepancies appear at larger

Mach number than at the previous roll angle. The pitching moment results from DREV follow the overall trend demonstrated by the results of Ref. 5, but the agreement between the two sets has definitely decreased since Fig. 13. At Mach numbers above 2.5, the difference between the two curves increases rapidly.

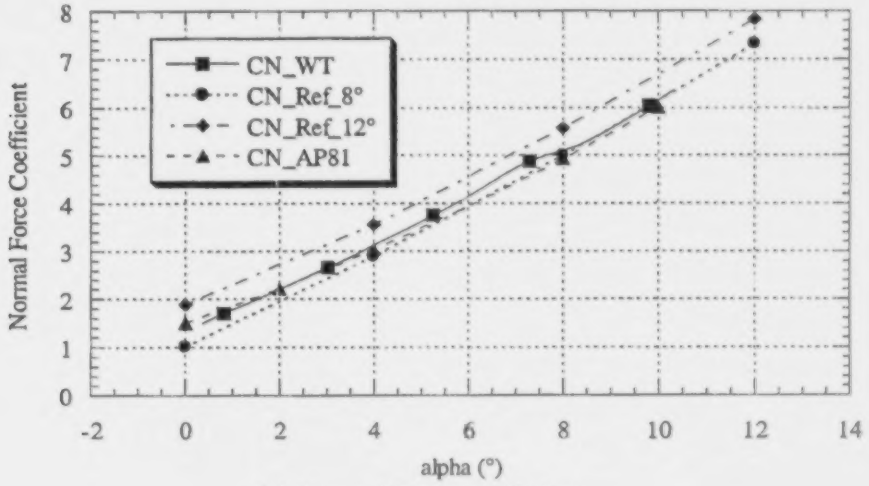

(a) Normal force coefficient

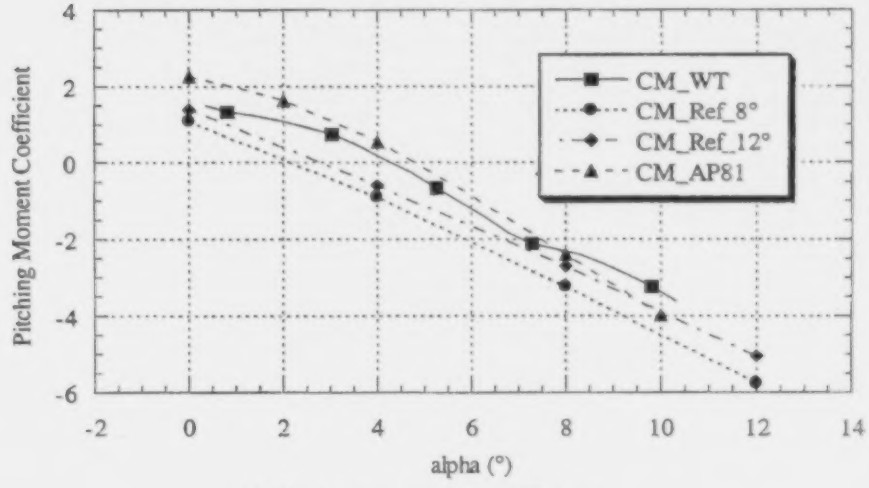

b) Pitching moment coefficient

FIGURE 16 – Aerodynamic coefficients for the F4 configuration at Mach 3.0 at 0° roll and with +10° on the wings

Figures 16 a) and b) show the same coefficients (normal force and pitching moment) as presented previously, but with the control wings at an angle of incidence. The wings of the missile have been positioned at an angle of incidence of 10°, and the missile pitched in the wind tunnel from -10° to +10°. Results from AP-81 were also generated for this case. From the AIM-7F reference, it was necessary to use values at 8° and 12° of

incidence on the wings, as results for 10° incidence did not exist. For the normal force, the actual results for 8° are lower and for 12° are higher than the wind tunnel and the AP-81 results, as expected. The general trends are well predicted, and the values compare well. For the pitching moment, the results are not as precise as in the previous case. The general trends of the experimental curves are well followed by the DREV and the AP-81 results. However, the results from the DREV wind tunnel are larger than both the 8° and the 12° results, and are over-predicted by the AP-81 results. Interestingly enough, the accuracy shown by the results for this 0° roll configuration is still better than that shown in Fig. 15 (45° roll configuration). This seems to confirm the trend identified previously on the decrease in the accuracy of the results for the 45° roll configuration cases when compared to the 0° roll configuration cases.

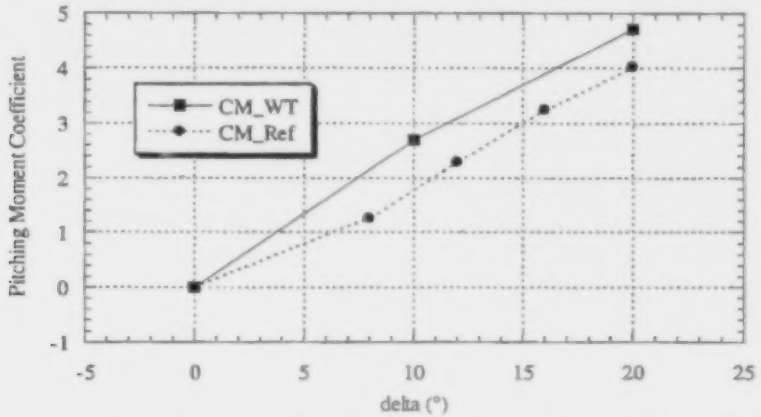

FIGURE 17 – Pitching moment coefficient for the F4 configuration at Mach 2.5 at 0° roll for variations in wing deflection

Finally, Fig. 17 shows the pitching moment coefficient in terms of wing deflections for a 0° angle of incidence of the missile body at Mach 2.5. Again, a constant differential exists between the two curves, but the general trends demonstrated by the results from actual values are well reproduced by the wind tunnel data.

Additional results from this experiment have been tabulated and are presented in Appendix C. A larger set of graphical results has also been included in Appendix D. These figures only provide results for the present wind tunnel experiment, without any comparisons to semi-empirical or other experimental values.

5.0 CONCLUSIONS AND RECOMMENDATIONS

The driving force behind this investigation was composed of two specific goals. The first one was to generate an aerodynamic coefficient database on a known missile body for future use in the reaction jet program. The second one was to validate the accuracy of DREV's wind tunnel in the study of high l/d models with large appendages.

With the use of the several configurations (F1 to F5), a complete aerodynamic coefficient database was generated for the model, over the range of Mach numbers from 1.5 to 4.0, and for angles of incidence from -10° to + 10°. Additionally, data involving wing deflections were also generated for the same Mach number range, over the same model incidence range, for deflection angles up to 20°. Thus, a fairly comprehensive database was generated by this experiment. This memorandum introduces a substantial cross-sectional review of some of these results, but it does not pretend to present all of the results. It is assumed that the amount of data presented in this document is sufficient to achieve the goals outlined in the introduction.

Comparisons with actual AIM-7F data have shown that DREV's Trisonic Wind Tunnel can provide results comparing well with actual missile bodies. Thus, high l/d bodies with large appendages can successfully be tested in this facility.

One of the recommendations would be to perform a few additional tests at a later date when a suitable ABLE balance becomes available, in order to generate the missing drag coefficient values to populate the data base.

6.0 ACKNOWLEDGEMENTS

The author would like to thank Mr. B. Girard for his work in the development of the model and of the testing methodology. The author would also like to thank Messrs. R. Bilodeau and M. Boivin for their assistance in the experimental work. The excellent work of the Prototype Group's staff in the fabrication of the models is also greatly acknowledged.

7.0 REFERENCES

1. Fournier, É. Y. and Jeffrey, A. J., "A Computational Fluid Dynamic Analysis of Freestream-Jet Interaction with Application to Reaction-Jet Control on Supersonic Missile Bodies," DREV TM-9418, October 1994, UNCLASSIFIED

2. Fournier, É. Y., "Boundary Layer Survey on a Model of a Sparrow AIM-7M Missile in the DREV Trisonic Wind Tunnel", DREV TM-1999-088, 1999, UNCLASSIFIED

3. Vittecoq, P., Bourassa, P.A. and Laneville, A., "Développement de balances extensométriques de type interne à cinq composantes", Université de Sherbrooke, Final report, Contract # 19-SD-97701-6-1783A, April 1988.

4. Mason, L., Devan, L., Moore, F.G. and McMillan, D., "Aerodynamic Design Manual for Tactical Weapons", Naval Surface Weapons Center, NSWC TR-81-156, July 1981, UNCLASSIFIED.

5. Joint Munitions Effectiveness Group, "Missile Simulation Computer Program for AIM-7F (U)", JTCG/ME, NAVAIR, March 1979.

6. Uselton, B.L. and Haberman, D.R., "Summary of Sting Interference Effects for Cone, Missile and Aircraft Configurations as Determined by Dynamic and Static Measurements", AIAA-82-1366, August 1982.

7. Hoerner, S. F., "Fluid-Dynamic Drag", Washington DC, August 1957.

APPENDIX A

Testing Schedule

AERODYNAMIC COEFFICIENT MEASUREMENTS

Sparrow model

NOMENCLATURE

Model at 45°

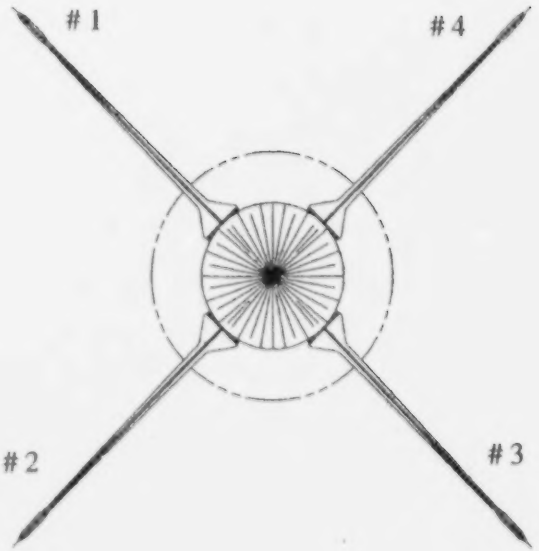

Model at 0°

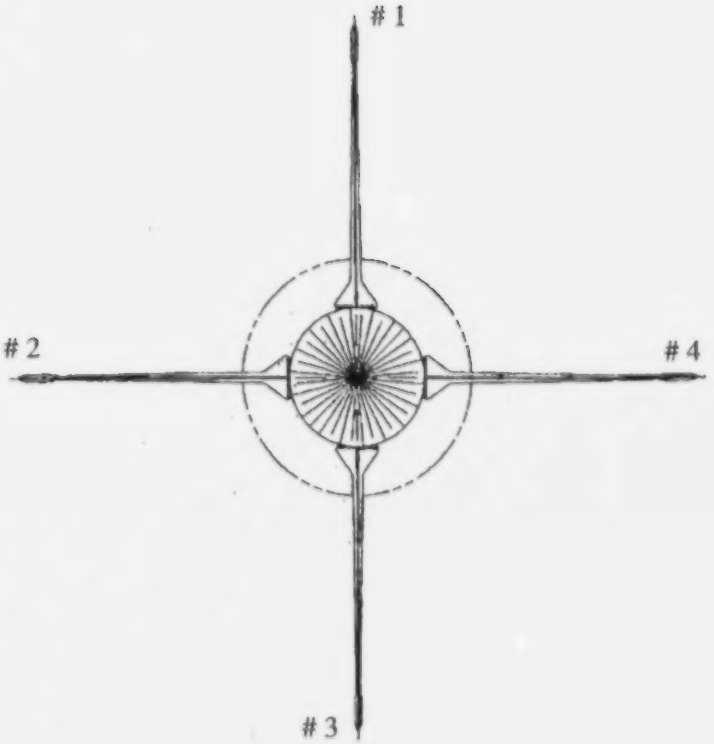

Note : Looking downstream (at the nose of the missile)

Wings and fins angle nomenclature

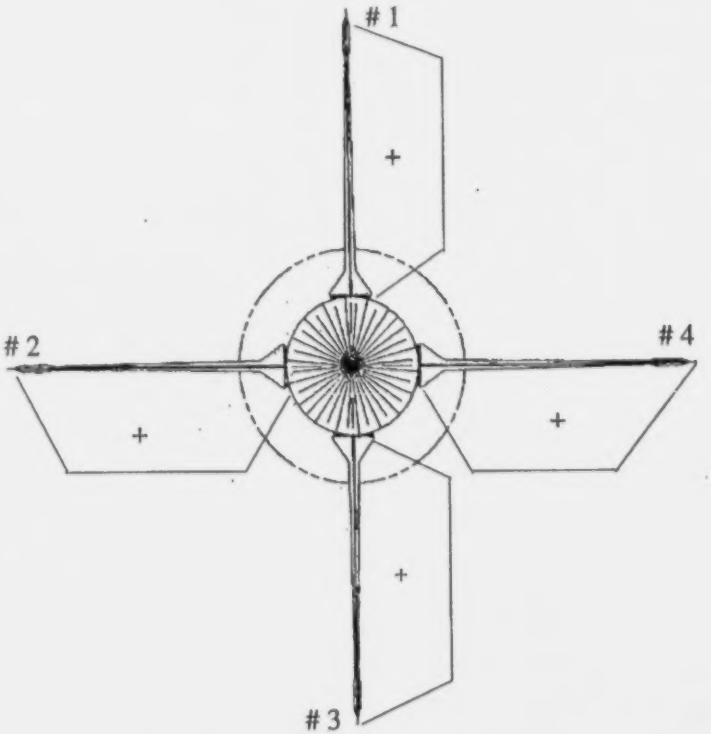

Reference point for moment: (C_m): 73 inches from nose of missile (body diameter 8 inches) : 9.125 body diameter from nose (or 8.579 body diameter from base).

NOMENCLATURE FROM SPARROW REPORT

Directions and angles

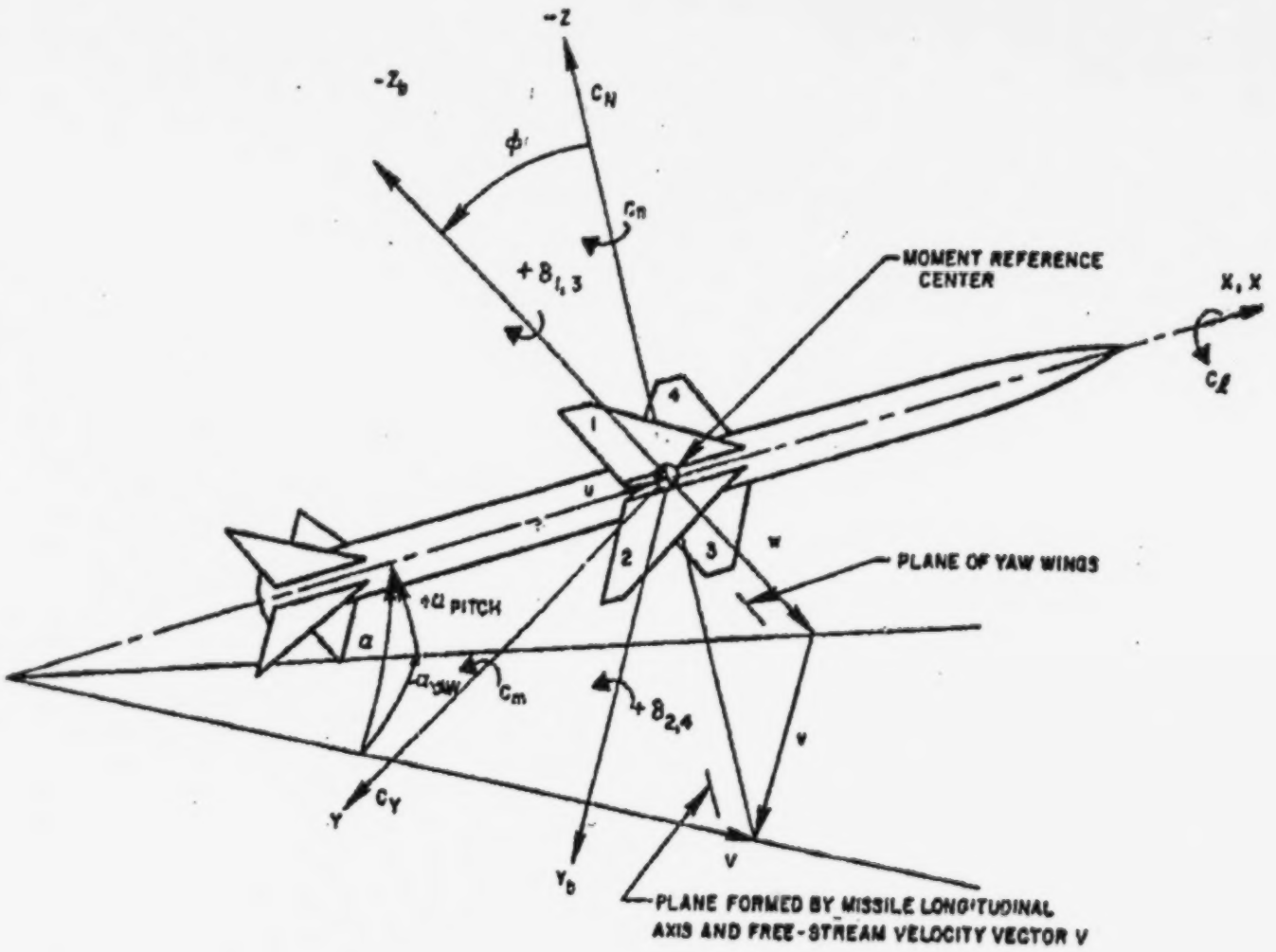

AERODYNAMIC COEFFICIENT MEASUREMENTS : Mach 2.0 Data

Test Number	Run Number	Configuration	Sweep Angles	Model Roll Angle	Mach Number
F1.20.+.00.1	R6456	Body	-10° to +10°	0° (+)	2.0
F1.20.x.00.1	R6457	Body	-10° to +10°	45° (x)	2.0
F2.20.+.00.1	R6442	Body + control fins	-10° to +10°	0° (+)	2.0
F2.20.+.00.2	R6443	Body + control fins	-10° to +10°	0° (+)	2.0
F2.20.x.00.1	R6440	Body + control fins	-10° to +10°	45° (x)	2.0
F2.20.x.00.2	R6441	Body + control fins	-10° to +10°	45° (x)	2.0
F2.20.90.00.1	R6446	Body + control fins	-10° to +10°	90°	2.0
F2.20.135.00.1	R6448	Body + control fins	-10° to +10°	135°	2.0
F2.20.180.00.1	R6447	Body + control fins	-10° to +10°	180°	2.0
F3.20.+.00.1	R6452	Body + tail fins	-10° to +10°	0° (+)	2.0
F3.20.+.00.2	R6453	Body + tail fins	-10° to +10°	0° (+)	2.0
F3.20.x.00.1	R6449	Body + tail fins	-10° to +10°	45° (x)	2.0
F3.20.x.00.2	R6450	Body + tail fins	-10° to +10°	45° (x)	2.0
F3.20.90.00.1	R6454	Body + tail fins	-10° to +10°	90°	2.0
F3.20.135.00.1	R6451	Body + tail fins	-10° to +10°	135°	2.0
F3.20.180.00.1	R6455	Body + tail fins	-10° to +10°	180°	2.0
F4.20.+.00.1	R6436	Body + control fins + tail fins	-10° to +10°	0° (+)	2.0
F4.20.+.00.2	R6437	Body + control fins + tail fins	-10° to +10°	0° (+)	2.0
F4.20.x.00.1	R6438	Body + control fins + tail fins	-10° to +10°	45° (x)	2.0
F4.20.x.00.2	R6439	Body + control fins + tail fins	-10° to +10°	45° (x)	2.0
F5.20.x.00.1	R6444	Body + control fins + tail fins + fittings	-10° to +10°	45° (x)	2.0
F5.20.x.00.2	R6445	Body + control fins + tail fins + fittings	-10° to +10°	45° (x)	2.0

AERODYNAMIC COEFFICIENT MEASUREMENTS : Mach 2.5 Data

Test Number	Run Number	Configuration	Sweep Angles	Model Roll Angle	Mach Number
F1.25.+.00.1	R6404	Body	-10° to +10°	0° (+)	2.5
F1.25.x.00.1	R6403	Body	-10° to +10°	45° (x)	2.5
F2.25.+.00.1	R6411	Body + control fins	-10° to +10°	0° (+)	2.5
F2.25.+.00.2	R6412	Body + control fins	-10° to +10°	0° (+)	2.5
F2.25.x.00.1	R6409	Body + control fins	-10° to +10°	45° (x)	2.5
F2.25.x.00.2	R6410	Body + control fins	-10° to +10°	45° (x)	2.5
F3.25.+.00.1	R6405	Body + tail fins	-10° to +10°	0° (+)	2.5
F3.25.+.00.2	R6406	Body + tail fins	-10° to +10°	0° (+)	2.5
F3.25.x.00.1	R6407	Body + tail fins	-10° to +10°	45° (x)	2.5
F3.25.x.00.2	R6408	Body + tail fins	-10° to +10°	45° (x)	2.5
F4.25.+.00.1	R6413	Body + control fins + tail fins	-10° to +10°	0° (+)	2.5
F4.25.+.00.2	R6414	Body + control fins + tail fins	-10° to +10°	0° (+)	2.5
F4.25.x.00.1	R6415	Body + control fins + tail fins	-10° to +10°	45° (x)	2.5
F4.25.x.00.2	R6416	Body + control fins + tail fins	-10° to +10°	45° (x)	2.5
F5.25.x.00.1	R6421	Body + control fins + tail fins + fittings	-10° to +10°	45° (x)	2.5
F5.25.x.00.2	R6422	Body + control fins + tail fins + fittings	-10° to +10°	45° (x)	2.5
F5.25.x.00.3	R6423	Body + control fins + tail fins + fittings	-10° to +10°	45° (x)	2.5

AERODYNAMIC COEFFICIENT MEASUREMENTS : Mach 3.0 Data

Test Number	Run Number	Configuration	Sweep Angles	Model Roll Angle	Mach Number
F1.30.+.00.1	R6401	Body	-10° to +10°	0° (+)	3.0
F1.30.x.00.1	R6402	Body	-10° to +10°	45° (x)	3.0
F2.30.+.00.1	R6393	Body + control fins	-10° to +10°	0° (+)	3.0
F2.30.+.00.2	R6394	Body + control fins	-10° to +10°	0° (+)	3.0
F2.30.x.00.1	R6395	Body + control fins	-10° to +10°	45° (x)	3.0
F2.30.x.00.2	R6396	Body + control fins	-10° to +10°	45° (x)	3.0
F3.30.+.00.1	R6399	Body + tail fins	-10° to +10°	0° (+)	3.0
F3.30.+.00.2	R6400	Body + tail fins	-10° to +10°	0° (+)	3.0
F3.30.x.00.1	R6397	Body + tail fins	-10° to +10°	45° (x)	3.0
F3.30.x.00.2	R6398	Body + tail fins	-10° to +10°	45° (x)	3.0
F4.30.+.00.1	R6386	Body + control fins + tail fins	-10° to +10°	0° (+)	3.0
F4.30.+.00.2	R6387	Body + control fins + tail fins	-10° to +10°	0° (+)	3.0
F4.30.x.00.1	R6388	Body + control fins + tail fins	-10° to +10°	45° (x)	3.0
F4.30.x.00.2	R6389	Body + control fins + tail fins	-10° to +10°	45° (x)	3.0
F5.30.x.00.1	R6390	Body + control fins + tail fins + fittings	-10° to +10°	45° (x)	3.0
F5.30.x.00.2	R6391	Body + control fins + tail fins + fittings	-10° to +10°	45° (x)	3.0
F5.30.x.00.3	R6392	Body + control fins + tail fins + fittings	-10° to +10°	45° (x)	3.0

AERODYNAMIC COEFFICIENT MEASUREMENTS : Mach 3.5 Data

Test Number	Run Number	Configuration	Sweep Angles	Model Roll Angle	Mach Number
F1.35.+.00.1	R6216	Body	-10° to +10°	0° (+)	3.5
F1.35.x.00.1	R6221	Body	-10° to +10°	45° (x)	3.5
F2.35.+.00.1	R6354	Body + control fins	-10° to +10°	0° (+)	3.5
F2.35.+.00.2	R6355	Body + control fins	-10° to +10°	0° (+)	3.5
F2.35.x.00.1	R6356	Body + control fins	-10° to +10°	45° (x)	3.5
F2.35.x.00.2	R6357	Body + control fins	-10° to +10°	45° (x)	3.5
F3.35.+.00.1	R6361	Body + tail fins	-10° to +10°	0° (+)	3.5
F3.35.+.00.2	R6362	Body + tail fins	-10° to +10°	0° (+)	3.5
F3.35.x.00.1	R6363	Body + tail fins	-10° to +10°	45° (x)	3.5
F3.35.x.00.2	R6364	Body + tail fins	-10° to +10°	45° (x)	3.5
F4.35.+.00.1	R6345	Body + control fins + tail fins	-10° to +10°	0° (+)	3.5
F4.35.+.00.2	R6346	Body + control fins + tail fins	-10° to +10°	0° (+)	3.5
F4.35.x.00.1	R6347	Body + control fins + tail fins	-10° to +10°	45° (x)	3.5
F4.35.x.00.2	R6348	Body + control fins + tail fins	-10° to +10°	45° (x)	3.5
F5.35.x.00.1	R6349	Body + control fins + tail fins + fittings	-10° to +10°	45° (x)	3.5
F5.35.x.00.2	R6350	Body + control fins + tail fins + fittings	-10° to +10°	45° (x)	3.5
F5.35.x.00.3	R6351	Body + control fins + tail fins + fittings	-10° to +10°	45° (x)	3.5

AERODYNAMIC COEFFICIENT MEASUREMENTS

Sparrow model with control wings and tail fins, no fittings (F4)

Control Wings at 0° and at Incidence Angles

Mach 1.5 Data

Test Number	Run Number	Configuration	Sweep Angles	Model Roll Angle	Wing Angle	Mach Number
F4.15.+.0.1	R6458	Body + control fins + tail fins	-10° to +10°	0° (+)	0°	1.5
F4.15.+.0.2	R6459	Body + control fins + tail fins	-10° to +10°	0° (+)	0°	1.5
F4.15.x.0.1	R6460	Body + control fins + tail fins	-10° to +10°	45° (x)	0°	1.5
F4.15.x.0.2	R6461	Body + control fins + tail fins	-10° to +10°	45° (x)	0°	1.5

AERODYNAMIC COEFFICIENT MEASUREMENTS

Sparrow model with control wings and tail fins, no fittings (F4)

Control Wings at Incidence Angles

Mach 2.0 Data

Test Number	Run Number	Configuration	Sweep Angles	Model Roll Angle	Wing Angle	Mach Number
F4.20.+.10.1	R6428	Body + control fins + tail fins	-10° to +10°	0° (+)	+10°	2.0
F4.20.+.10.2	R6429	Body + control fins + tail fins	-10° to +10°	0° (+)	+10°	2.0
F4.20.x.10.1	R6430	Body + control fins + tail fins	-10° to +10°	45° (x)	+10°	2.0
F4.20.x.10.2	R6431	Body + control fins + tail fins	-10° to +10°	45° (x)	+10°	2.0
F4.20.x.20.1	R6432	Body + control fins + tail fins	-10° to +10°	45° (x)	+20°	2.0
F4.20.x.20.2	R6433	Body + control fins + tail fins	-10° to +10°	45° (x)	+20°	2.0
F4.20.+.20.1	R6434	Body + control fins + tail fins	-10° to +10°	0° (+)	+20°	2.0
F4.20.+.20.2	R6435	Body + control fins + tail fins	-10° to +10°	0° (+)	+20°	2.0

AERODYNAMIC COEFFICIENT MEASUREMENTS

Sparrow model with control wings and tail fins, no fittings (F4)

Control Wings at Incidence Angles

Mach 2.5 Data

Test Number	Run Number	Configuration	Sweep Angles	Model Roll Angle	Wing Angle	Mach Number
F4.25.+.10.1	R6426	Body + control fins + tail fins	-10° to +10°	0° (+)	+10°	2.5
F4.25.+.10.2	R6427	Body + control fins + tail fins	-10° to +10°	0° (+)	+10°	2.5
F4.25.x.10.1	R6424	Body + control fins + tail fins	-10° to +10°	45° (x)	+10°	2.5
F4.25.x.10.2	R6425	Body + control fins + tail fins	-10° to +10°	45° (x)	+10°	2.5
F4.25.x.20.1	R6417	Body + control fins + tail fins	-10° to +10°	45° (x)	+20°	2.5
F4.25.x.20.2	R6418	Body + control fins + tail fins	-10° to +10°	45° (x)	+20°	2.5
F4.25.+.20.1	R6419	Body + control fins + tail fins	-10° to +10°	0° (+)	+20°	2.5
F4.25.+.20.2	R6420	Body + control fins + tail fins	-10° to +10°	0° (+)	+20°	2.5

AERODYNAMIC COEFFICIENT MEASUREMENTS

Sparrow model with control wings and tail fins, no fittings (F4)

Control Wings at Incidence Angles

Mach 3.0 Data

Test Number	Run Number	Configuration	Sweep Angles	Model Roll Angle	Wing Angle	Mach Number
F4.30.+.10.1	R6376	Body + control fins + tail fins	-10° to +10°	0° (+)	+10°	3.0
F4.30.+.10.2	R6377	Body + control fins + tail fins	-10° to +10°	0° (+)	+10°	3.0
F4.30.+.10.3	R6378	Body + control fins + tail fins	-10° to +10°	0° (+)	+10°	3.0
F4.30.+.10.4	R6379	Body + control fins + tail fins	-10° to +10°	0° (+)	+10°	3.0
F4.30.x.10.1	R6380	Body + control fins + tail fins	-10° to +10°	45° (x)	+10°	3.0
F4.30.x.10.2	R6381	Body + control fins + tail fins	-10° to +10°	45° (x)	+10°	3.0
F4.30.x.20.1	R6382	Body + control fins + tail fins	-10° to +10°	45° (x)	+20°	3.0
F4.30.x.20.2	R6383	Body + control fins + tail fins	-10° to +10°	45° (x)	+20°	3.0
F4.30.+.20.1	R6384	Body + control fins + tail fins	-10° to +10°	0° (+)	+20°	3.0
F4.30.+.20.2	R6385	Body + control fins + tail fins	-10° to +10°	0° (+)	+20°	3.0

AERODYNAMIC COEFFICIENT MEASUREMENTS

Sparrow model with control wings and tail fins, no fittings (F4)

Control Wings at Incidence Angles

Mach 3.5 Data

Test Number	Run Number	Configuration	Sweep Angles	Model Roll Angle	Wing Angle	Mach Number
F4.35.+.10.1	R6374	Body + control fins + tail fins	-10° to +10°	0° (+)	+10°	3.5
F4.35.+.10.2	R6375	Body + control fins + tail fins	-10° to +10°	0° (+)	+10°	3.5
F4.35.x.10.1	R6365	Body + control fins + tail fins	-10° to +10°	45° (x)	+10°	3.5
F4.35.x.10.2	R6372	Body + control fins + tail fins	-10° to +10°	45° (x)	+10°	3.5
F4.35.x.20.1	R6368	Body + control fins + tail fins	-10° to +10°	45° (x)	+20°	3.5
F4.35.x.20.2	R6369	Body + control fins + tail fins	-10° to +10°	45° (x)	+20°	3.5
F4.35.+.20.1	R6370	Body + control fins + tail fins	-10° to +10°	0° (+)	+20°	3.5
F4.35.+.20.2	R6371	Body + control fins + tail fins	-10° to +10°	0° (+)	+20°	3.5

AERODYNAMIC COEFFICIENT MEASUREMENTS

Sparrow model with control wings and tail fins, no fittings (F4)

Control Wings at 0° and at Incidence Angles

Mach 4.0 Data

Test Number	Run Number	Configuration	Sweep Angles	Model Roll Angle	Wing Angle	Mach Number
F4.40.+.0.1	R6464	Body + control fins + tail fins	-10° to +10°	0° (+)	0°	4.0
F4.40.+.0.2	R6465	Body + control fins + tail fins	-10° to +10°	0° (+)	0°	4.0
F4.40.x.0.1	R6462	Body + control fins + tail fins	-10° to +10°	45° (x)	0°	4.0
F4.40.x.0.2	R6463	Body + control fins + tail fins	-10° to +10°	45° (x)	0°	4.0

APPENDIX B

Selected Model Drawings

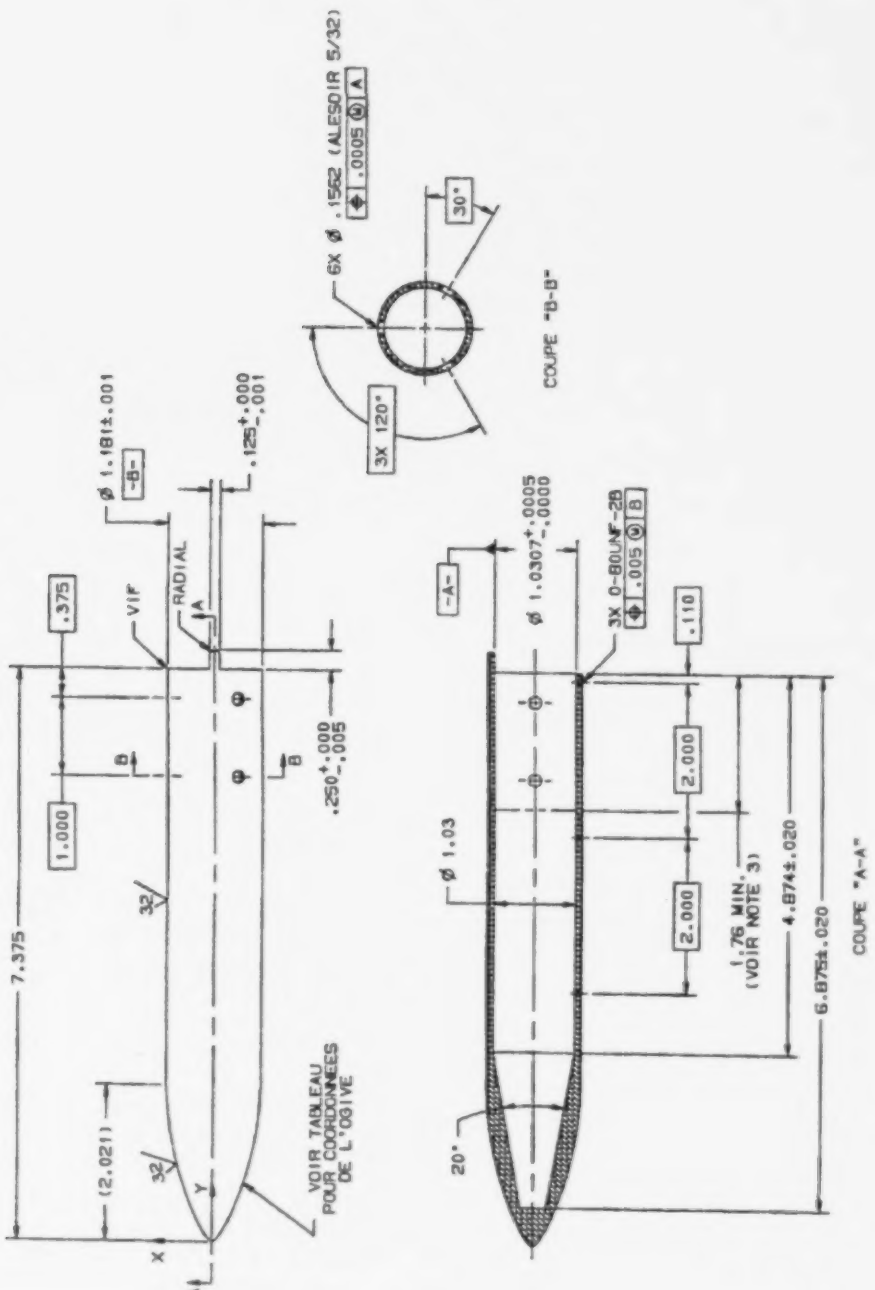

FIGURE B-1 – Sparrow model nose/forebody module (dimensions in inches)

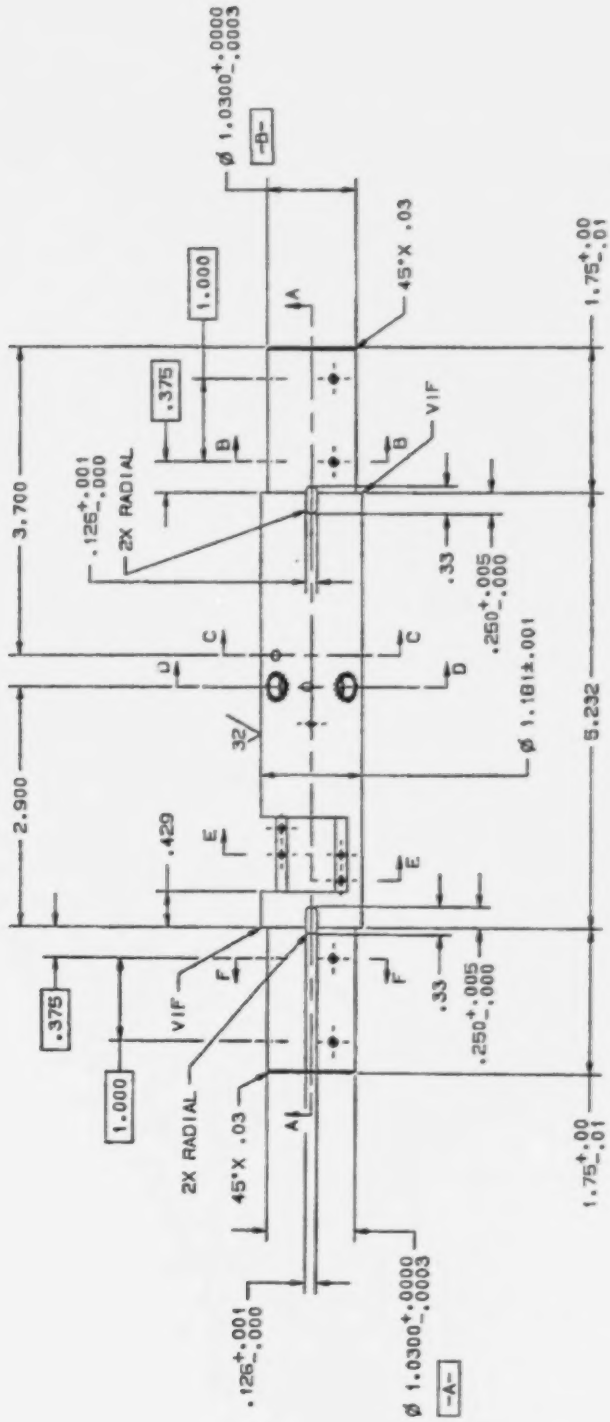

FIGURE B-2 – Sparrow model central body module, with control fins attachment holes (dimensions in inches)

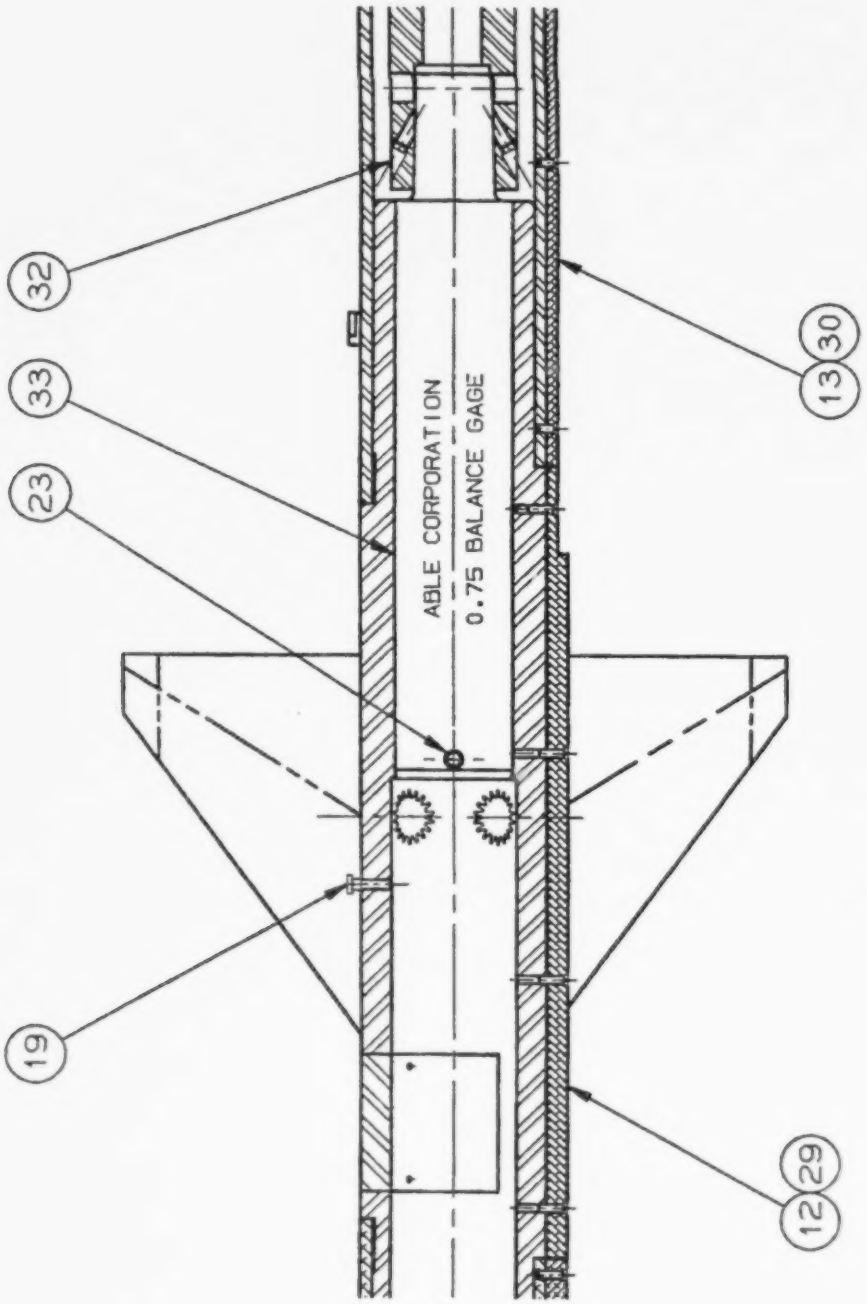

FIGURE B-3 – Sparrow model central body module used for aerodynamic studies (general arrangement)

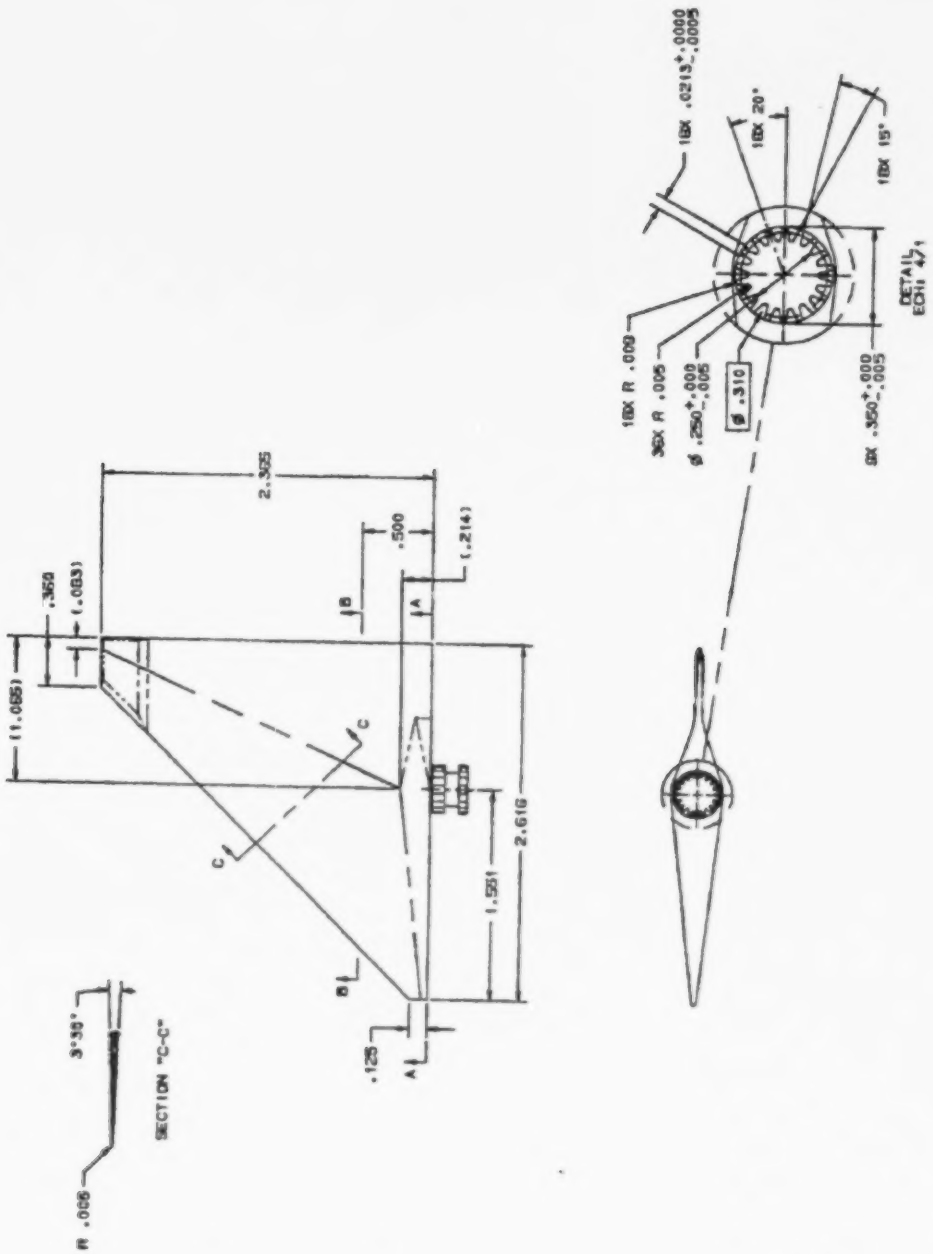

FIGURE B-4 – Sparrow model control fins (dimensions in inches)

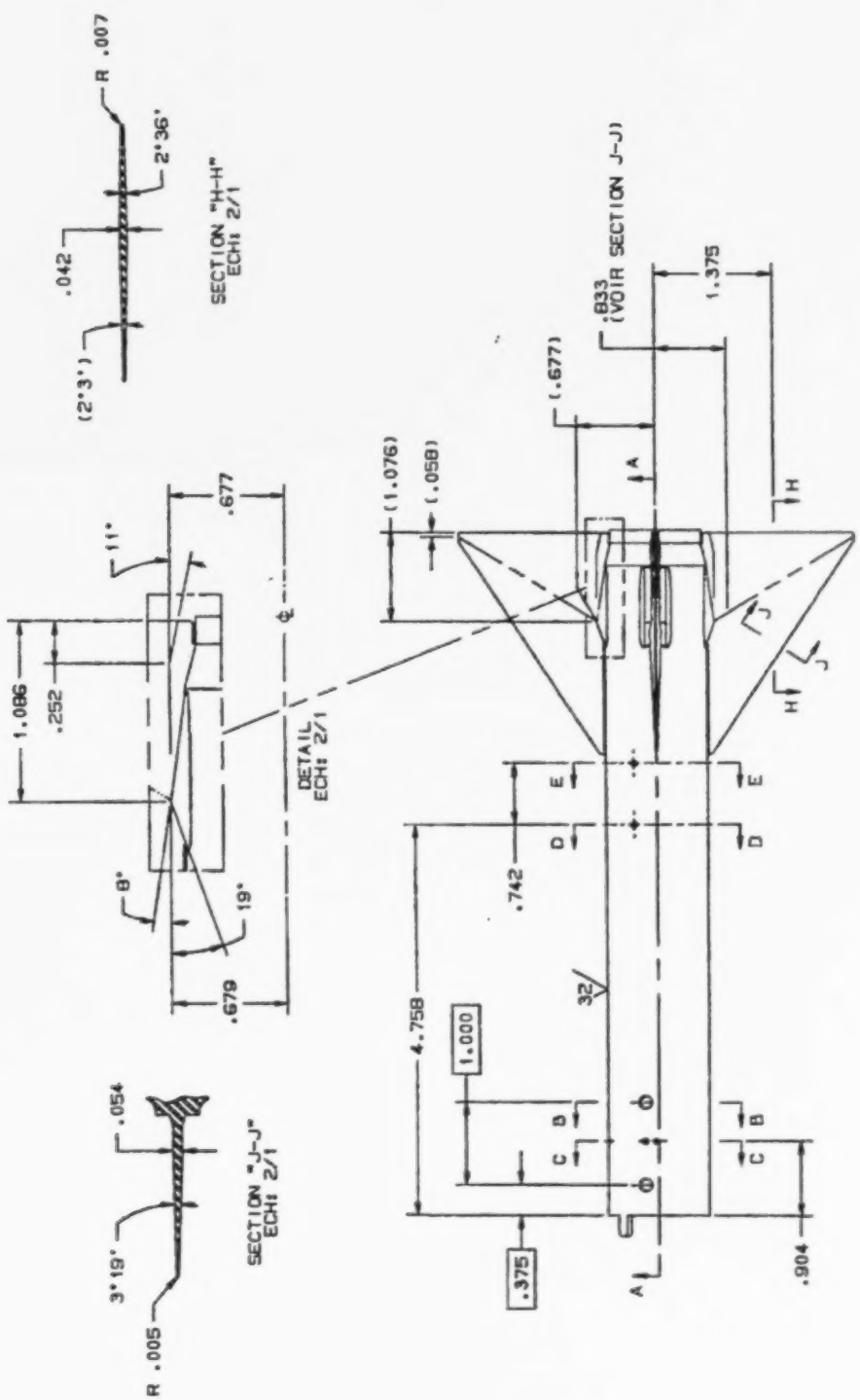

FIGURE B-5 – Sparrow model after-body module, with tail fins
(dimensions in inches)

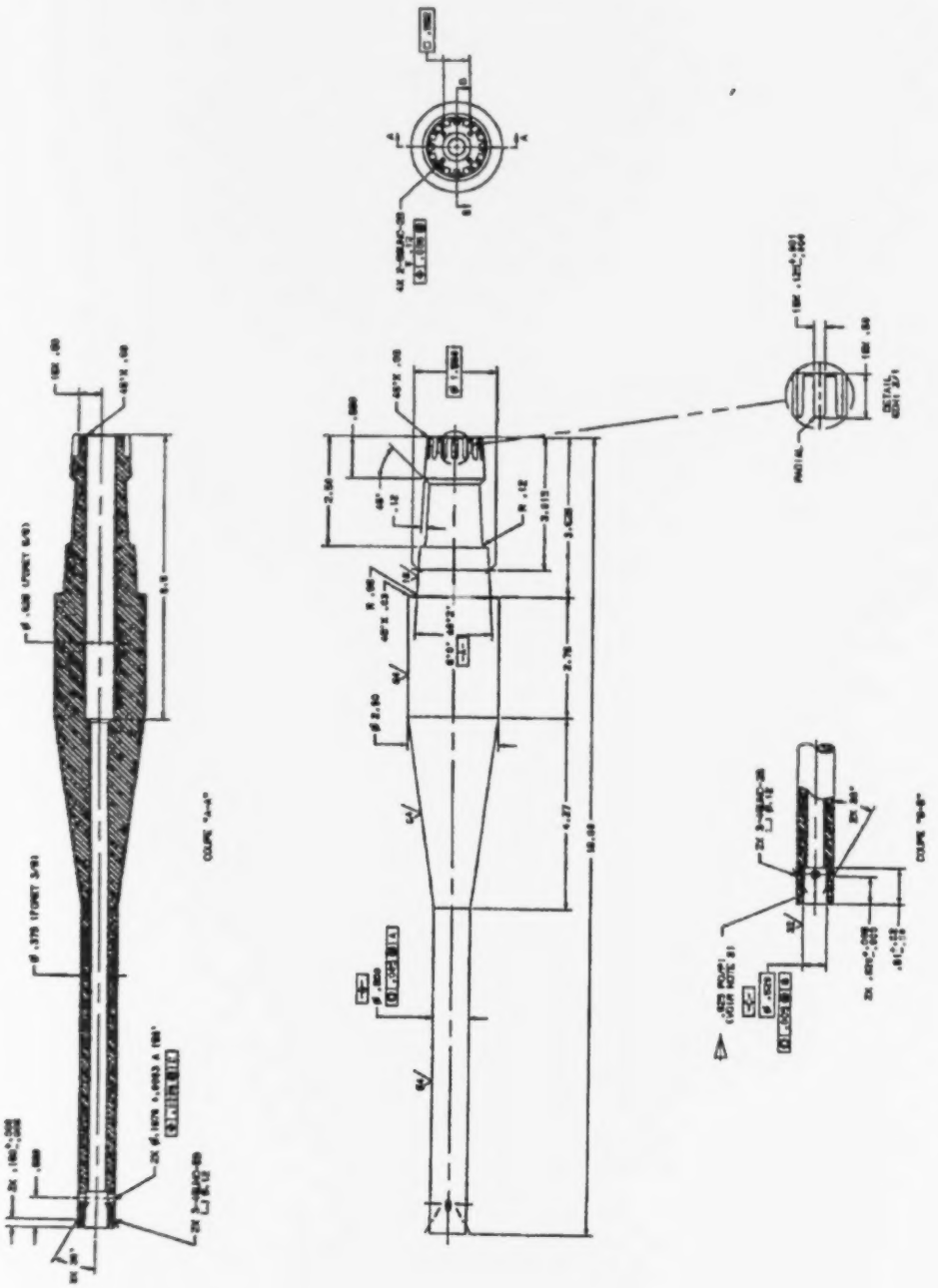

FIGURE B-6 – Balance (0.75 in) sting holder (dimensions in inches)

APPENDIX C

Tabulated Results

TABLE C-1

Aerodynamic Coefficients at Mach 1.5 for 3 Wing Deflections (0° Roll)

Coefficients	0°	10°	20°
CM_A	-57.149	-	-
CN_A	42.710	-	-
XCP_O	1.3381	-	-

TABLE C-2

Aerodynamic Coefficients at Mach 2.0 for 3 Wing Deflections (0° Roll)

Coefficients	0°	10°	20°
CM_A	-46.155	-49.511	-55.185
CN_A	33.264	33.622	33.247
XCP_O	1.3875	1.4726	1.6599

TABLE C-3

Aerodynamic Coefficients at Mach 2.5 for 3 Wing Deflections (0° Roll)

Coefficients	0°	10°	20°
CM_A	-35.027	-28.206	-15.861
CN_A	27.167	27.462	25.395
XCP_O	1.2893	1.0271	0.6246

TABLE C-4

Aerodynamic Coefficients at Mach 3.0 for 3 Wing Deflections (0° Roll)

Coefficients	0°	10°	20°
CM_A	-27.093	-20.578	-19.441
CN_A	24.448	24.992	25.445
XCP_O	1.1082	0.8234	0.7640

TABLE C-5

Aerodynamic Coefficients at Mach 3.5 for 3 Wing Deflections (0° Roll)

Coefficients	0°	10°	20°
CM_A	-23.047	-19.068	-17.924
CN_A	21.841	22.632	23.920
XCP_O	1.0552	0.8425	0.7493

TABLE C-6

Aerodynamic Coefficients at Mach 4.0 for 3 Wing Deflections (0° Roll)

Coefficients	0°	10°	20°
CM_A	-18.333	-	-
CN_A	19.865	-	-
XCP_O	0.9228	-	-

TABLE C-7

Aerodynamic Coefficients at Mach 1.5 for 3 Wing Deflections (45° Roll)

Coefficients	0°	10°	20°
CM_A	-50.963	-	-
CN_A	42.504	-	-
XCP_O	1.1990	-	-

TABLE C-8

Aerodynamic Coefficients at Mach 2.0 for 3 Wing Deflections (45° Roll)

Coefficients	0°	10°	20°
CM_A	-43.848	-58.087	-67.475
CN_A	33.467	33.703	36.294
XCP_O	1.3102	1.7235	1.8591

TABLE C-9

Aerodynamic Coefficients at Mach 2.5 for 3 Wing Deflections (45° Roll)

Coefficients	0°	10°	20°
CM_A	-33.976	-25.887	-18.492
CN_A	26.189	26.294	25.679
XCP_O	1.2973	0.9845	0.7201

TABLE C-10

Aerodynamic Coefficients at Mach 3.0 for 3 Wing Deflections (45° Roll)

Coefficients	0°	10°	20°
CM_A	-26.146	-21.421	-21.334
CN_A	24.176	25.059	25.574
XCP_O	1.0815	0.8548	0.8342

TABLE C-11

Aerodynamic Coefficients at Mach 3.5 for 3 Wing Deflections (45° Roll)

Coefficients	0°	10°	20°
CM_A	-23.760	-21.247	-20.946
CN_A	21.544	22.846	24.003
XCP_O	1.1029	0.9300	0.8727

TABLE C-12

Aerodynamic Coefficients at Mach 4.0 for 3 Wing Deflections (45° Roll)

Coefficients	0°	10°	20°
CM_A	-16.438	-	-
CN_A	19.251	-	-
XCP_O	0.8539	-	-

APPENDIX D

Results

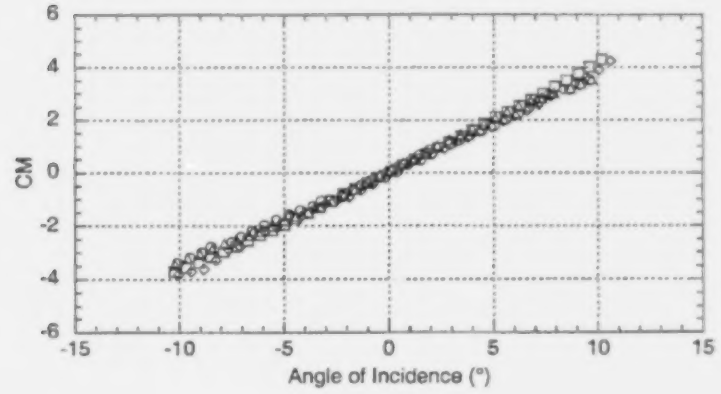

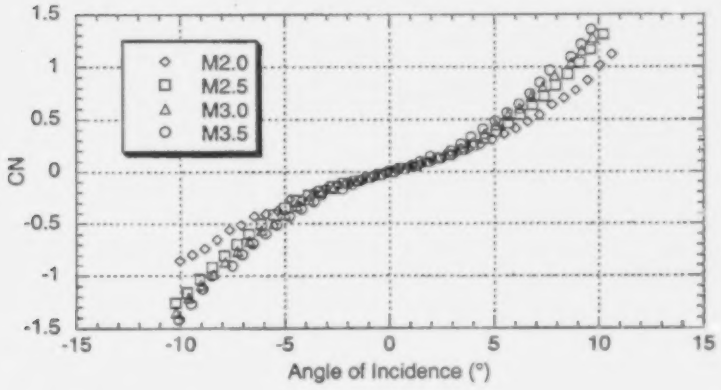

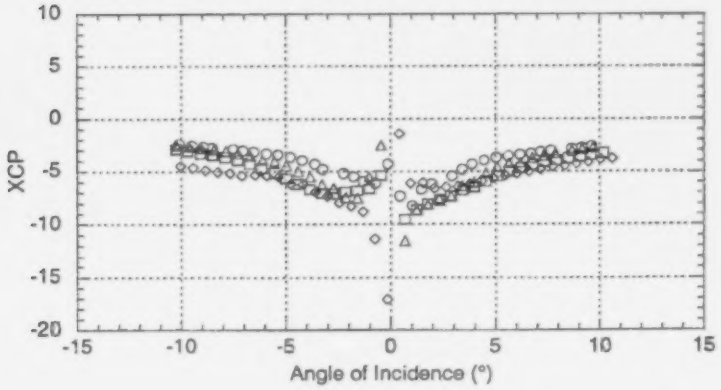

FIGURE D-1 – Configuration 1 aerodynamic coefficients (model roll orientation : 0°)

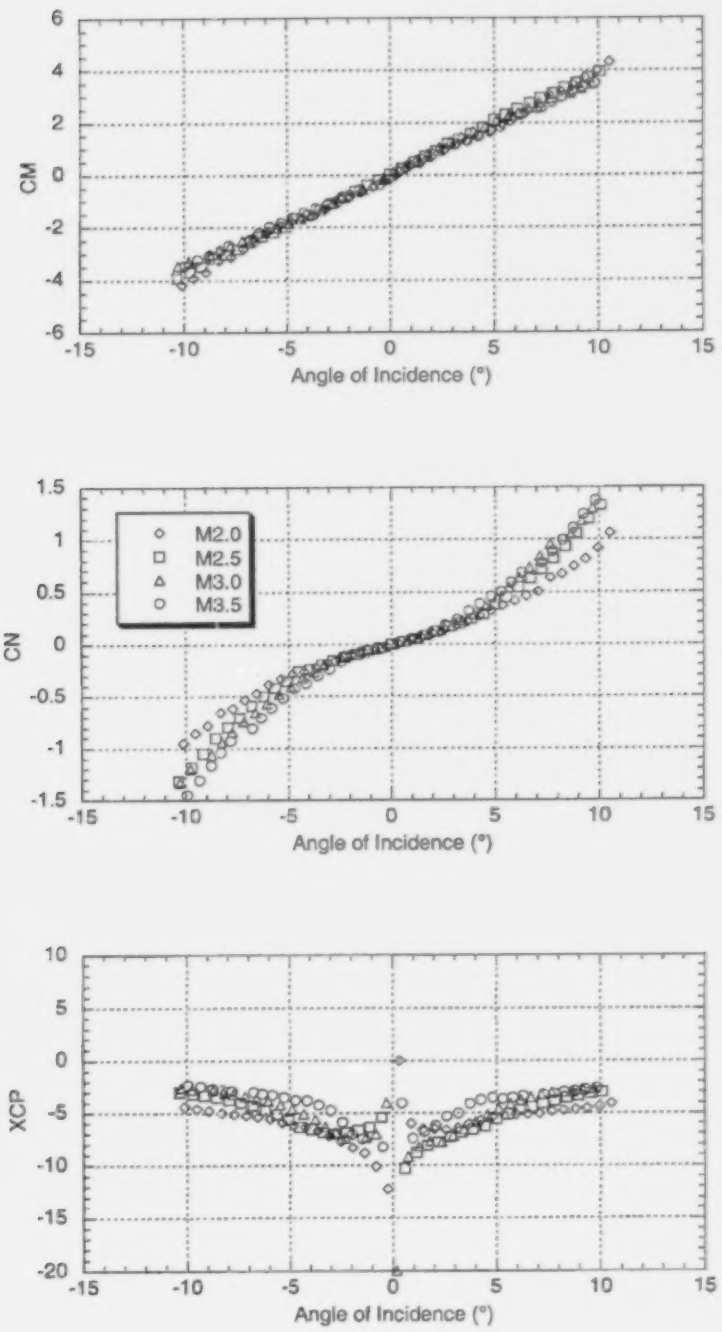

FIGURE D-2 – Configuration 1 aerodynamic coefficients (model roll orientation : 45°)

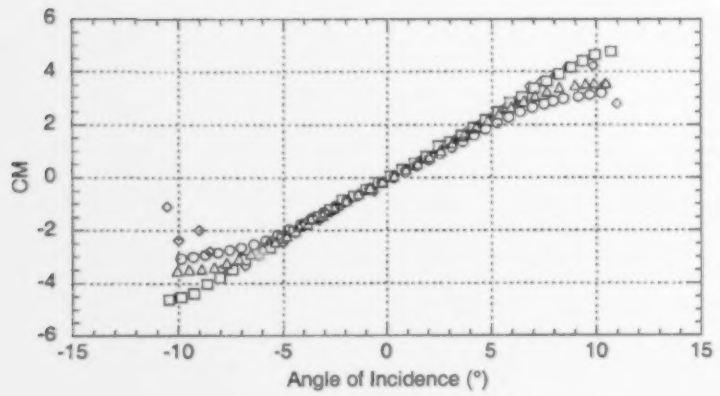

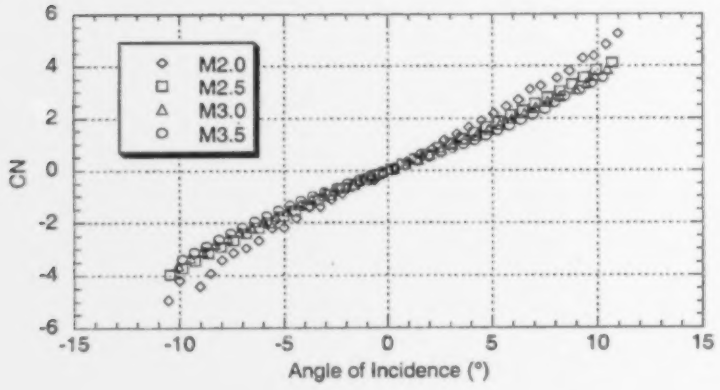

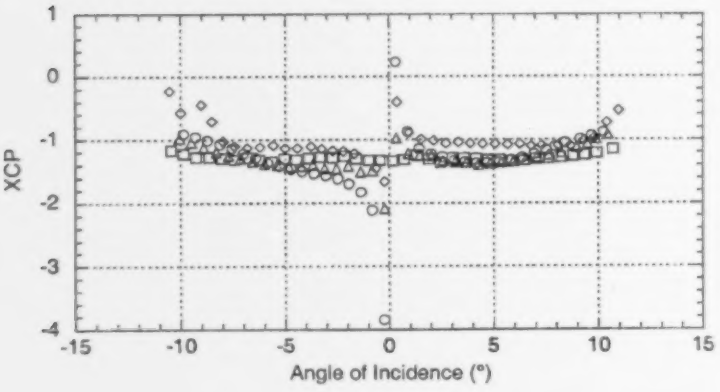

FIGURE D-3 – Configuration 2 aerodynamic coefficients (model roll orientation : 0°)

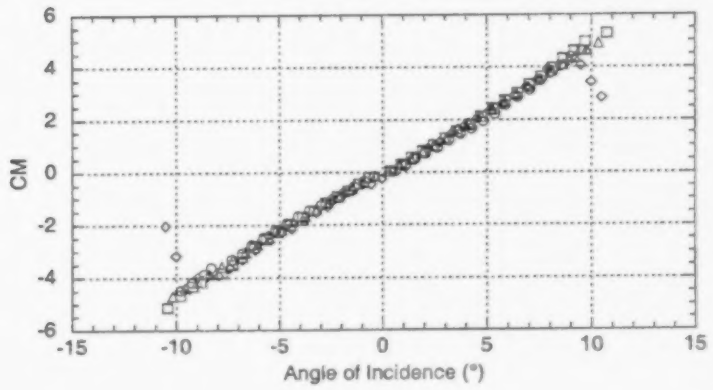

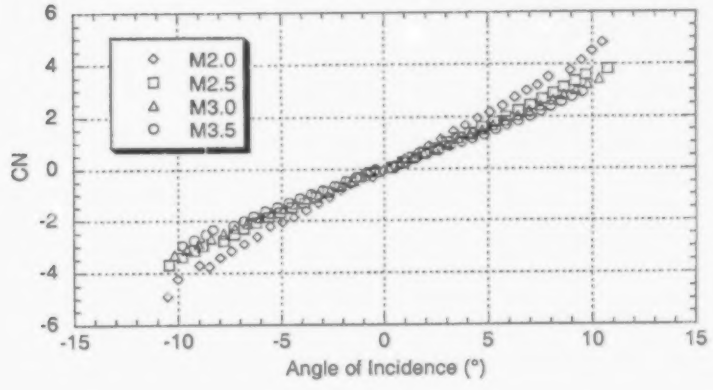

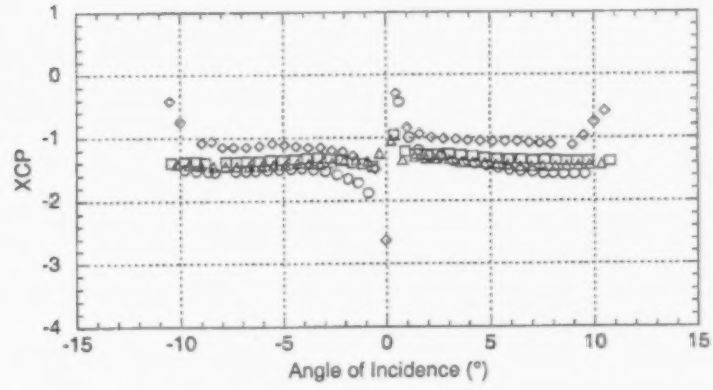

FIGURE D-4 – Configuration 2 aerodynamic coefficients (model roll orientation : 45°)

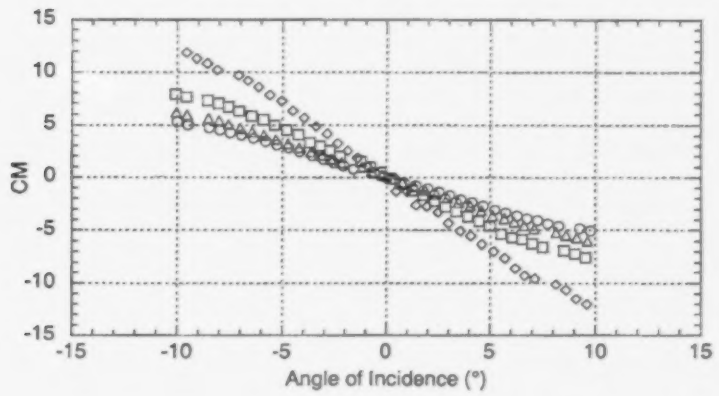

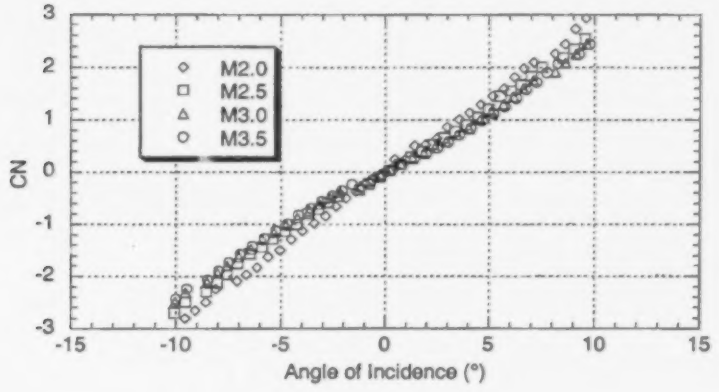

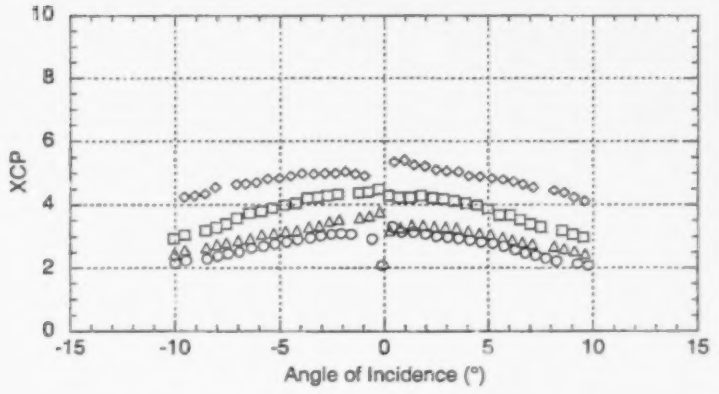

FIGURE D-5 – Configuration 3 aerodynamic coefficients (model roll orientation : 0°)

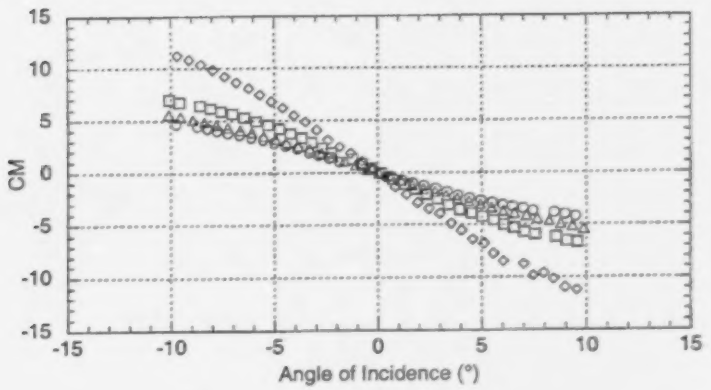

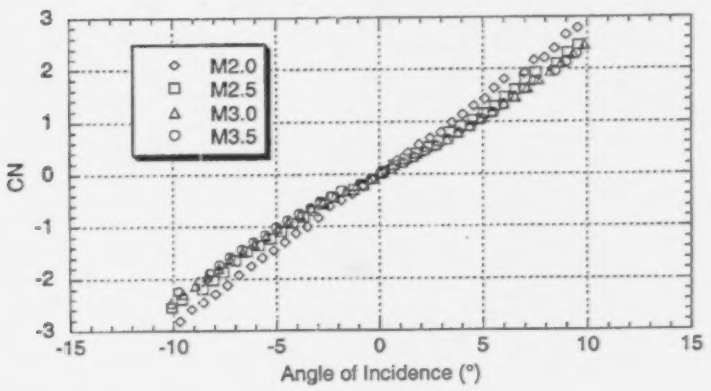

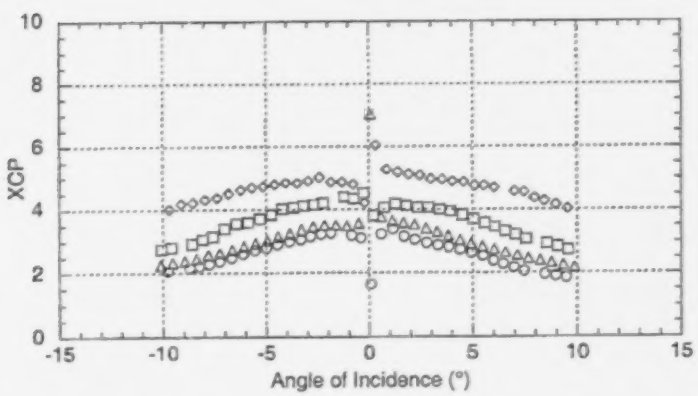

FIGURE D-6 – Configuration 3 aerodynamic coefficients (model roll orientation : 45°)

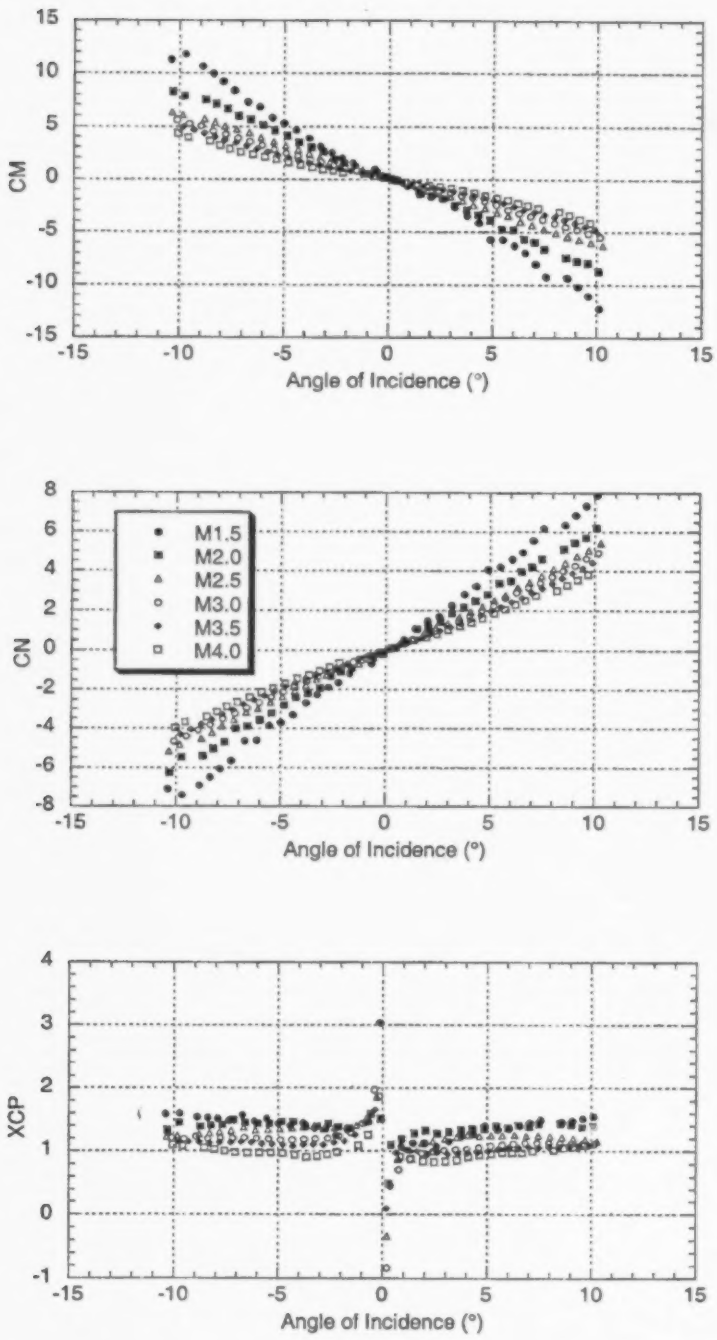

FIGURE D-7 – Configuration 4 aerodynamic coefficients (model roll orientation : 0°)

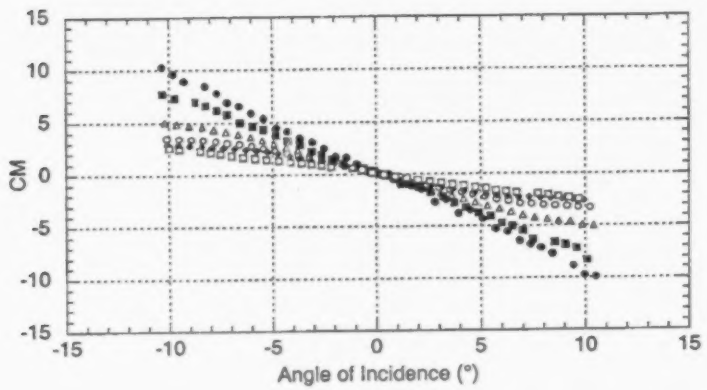

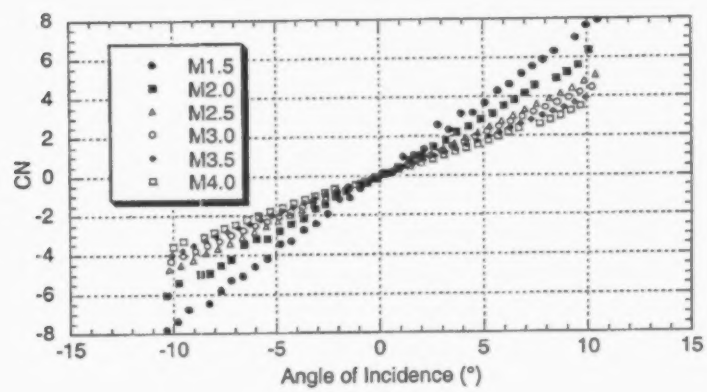

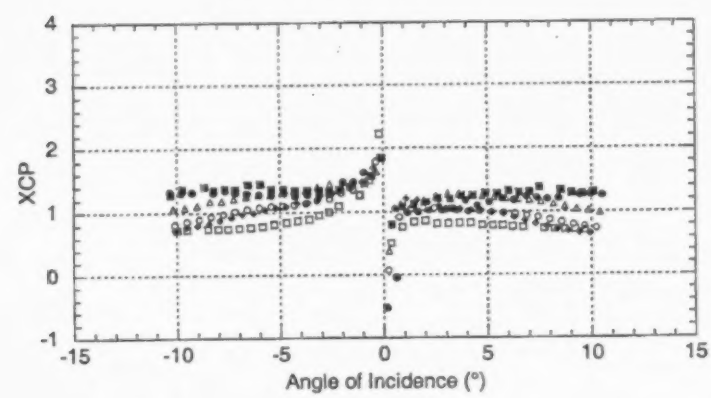

FIGURE D-8 – Configuration 4 aerodynamic coefficients (model roll orientation : 45°)

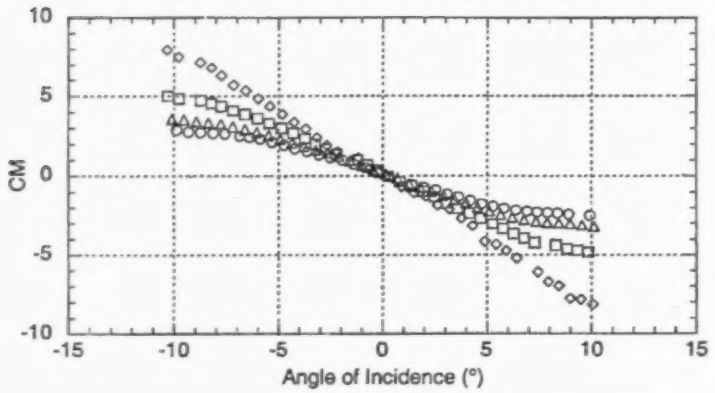

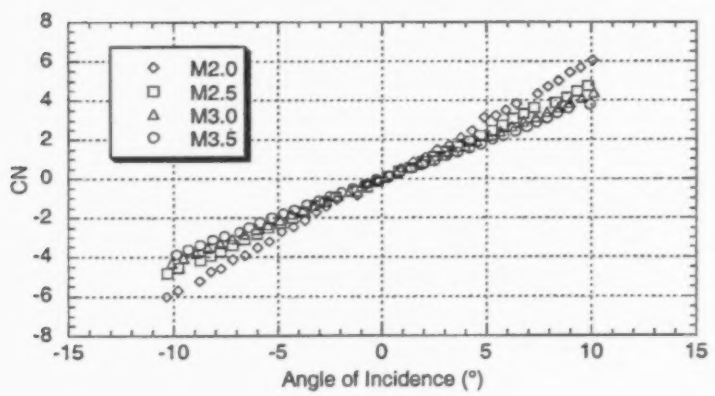

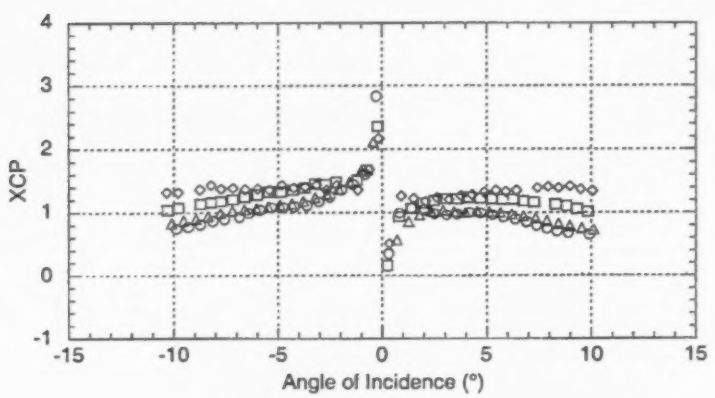

FIGURE D-9 – Configuration 5 aerodynamic coefficients (model roll orientation : 45°)

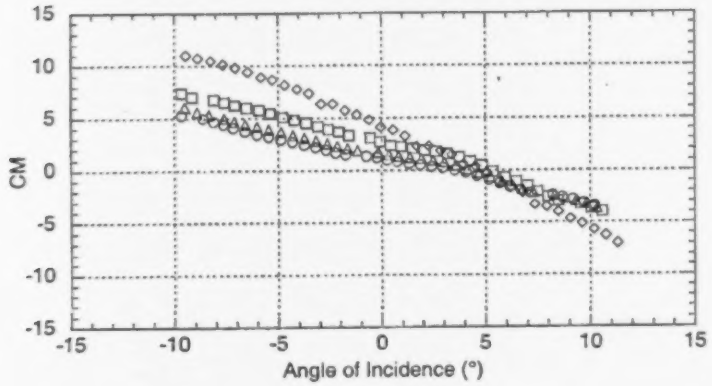

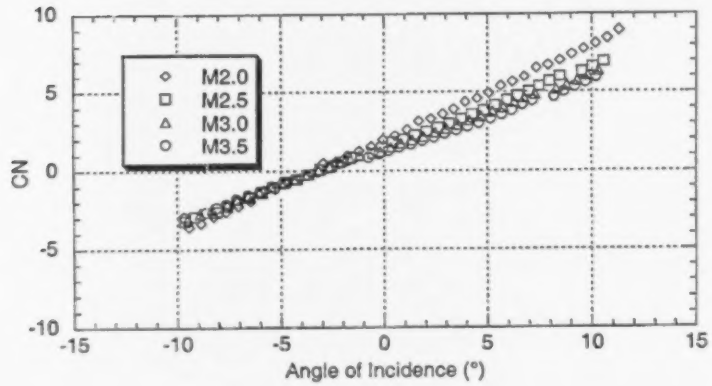

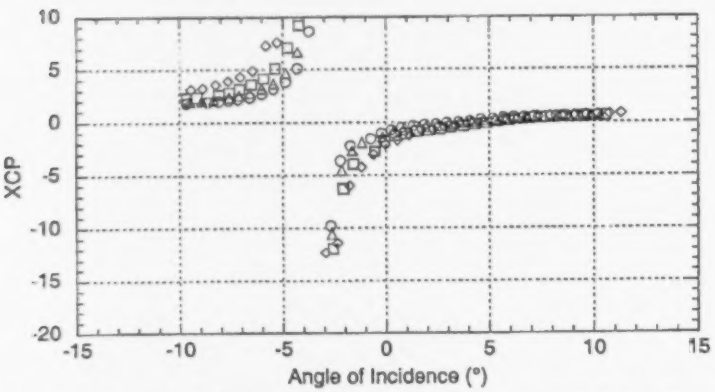

FIGURE D-10 – Configuration 4 aerodynamic coefficients (model roll orientation : 0°) with 10° wing deflection

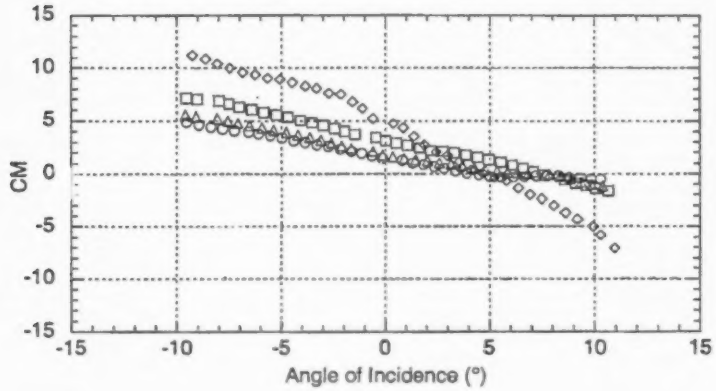

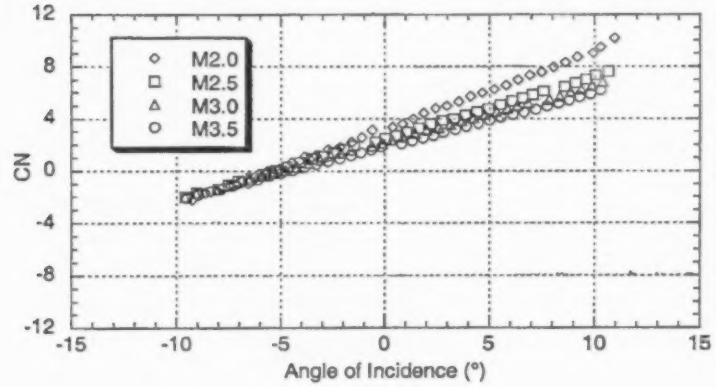

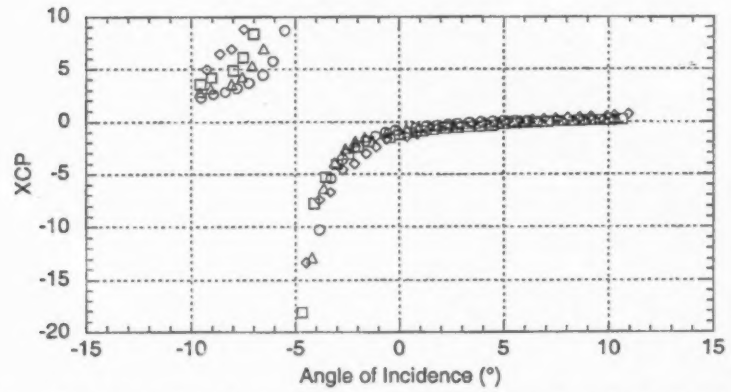

FIGURE D-11 – Configuration 4 aerodynamic coefficients (model roll orientation : 45°) with 10° wing deflection

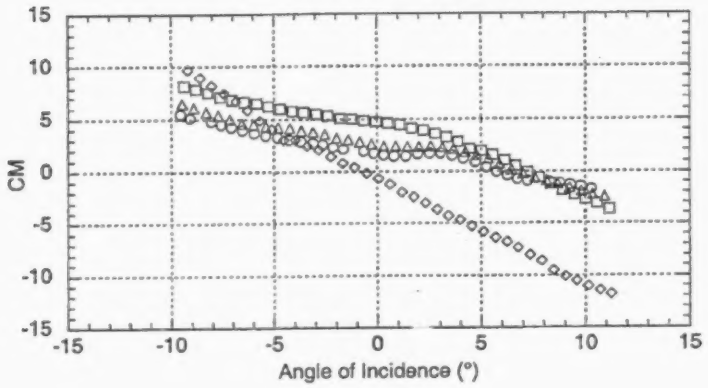

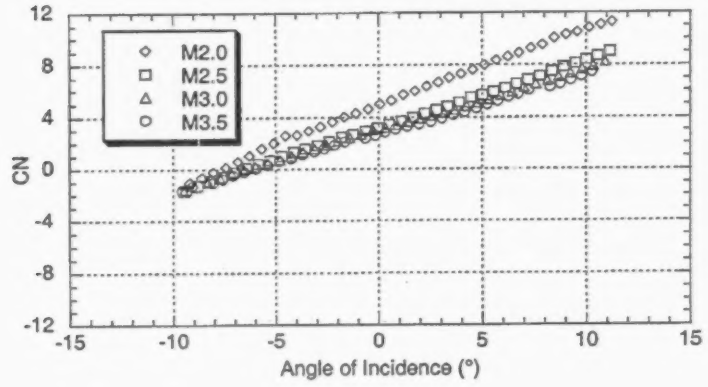

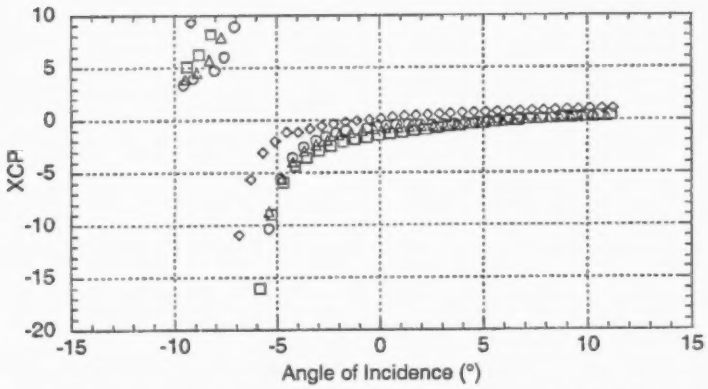

FIGURE D-12 – Configuration 4 aerodynamic coefficients (model roll orientation : 0°) with 20° wing deflection

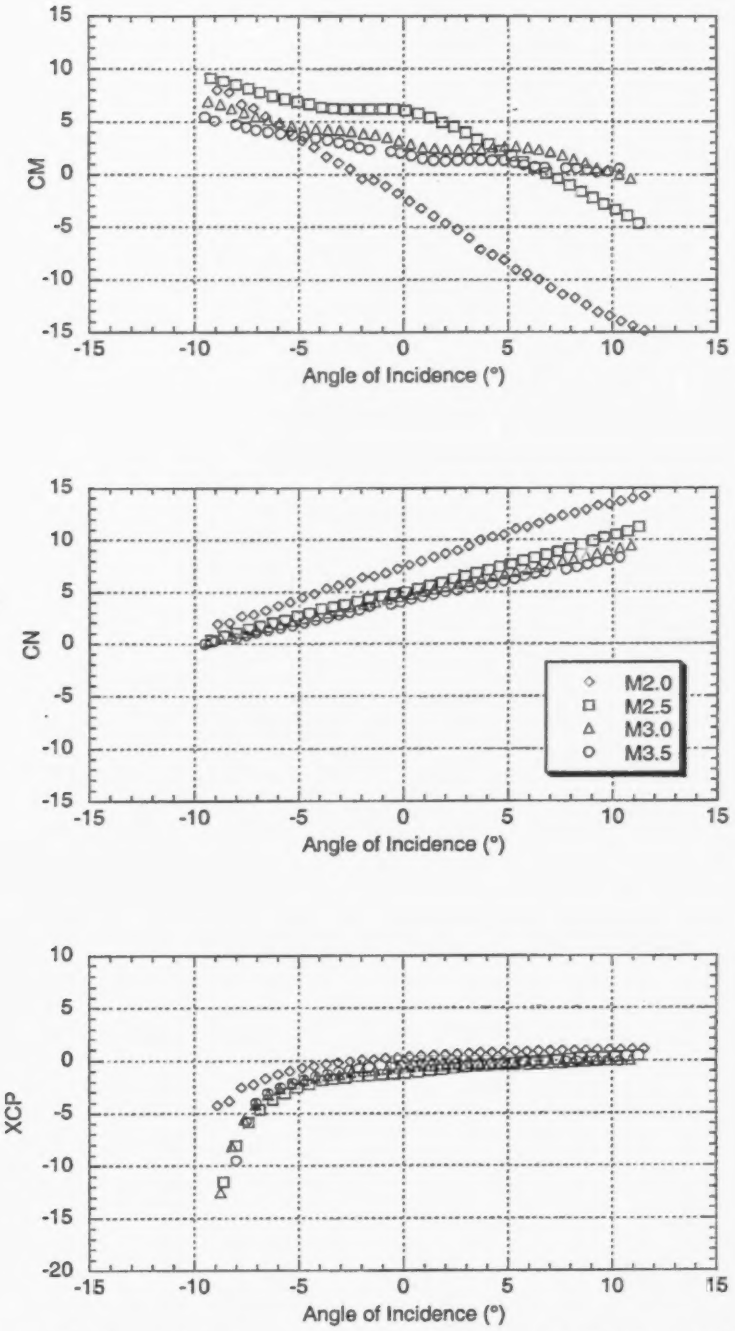

FIGURE D-13 – Configuration 4 aerodynamic coefficients (model roll orientation : 45°) with 20° wing deflection

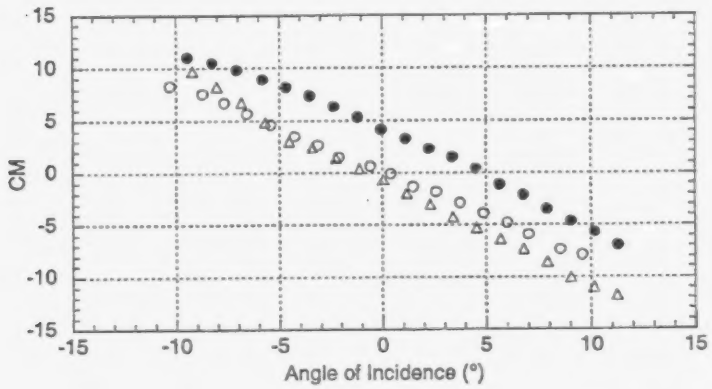

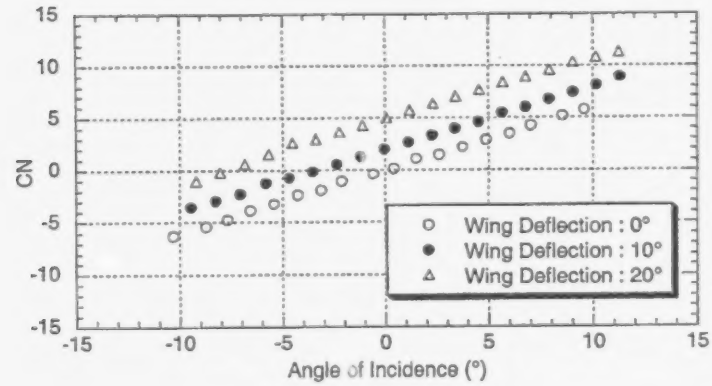

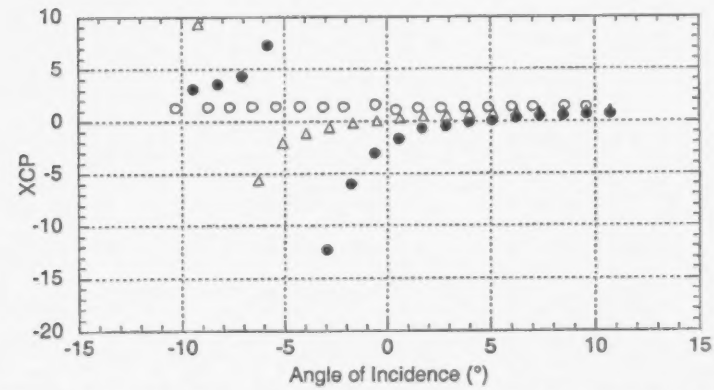

FIGURE D-14 – Configuration 4 aerodynamic coefficients at Mach 2.0
(model roll orientation : 0°)

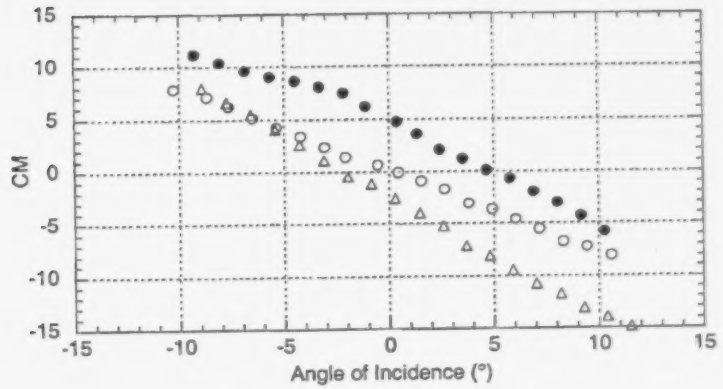

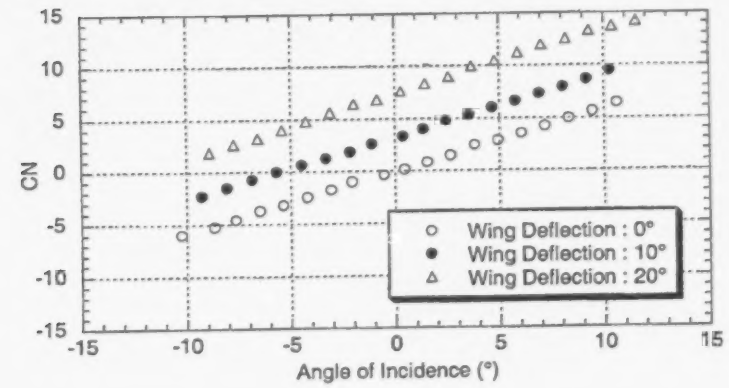

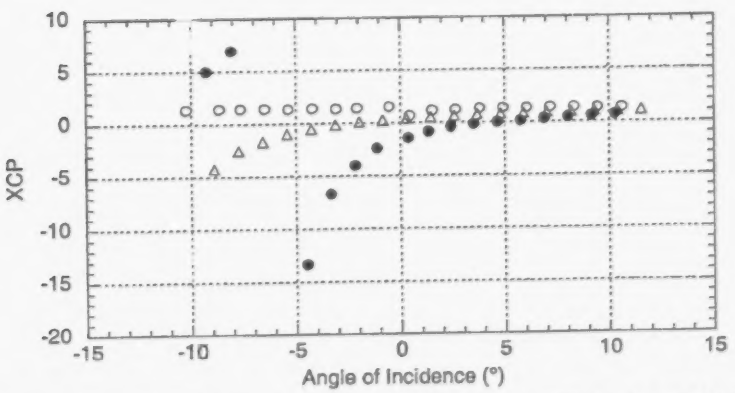

FIGURE D-15 – Configuration 4 aerodynamic coefficients at Mach 2.0 (model roll orientation : 45°)

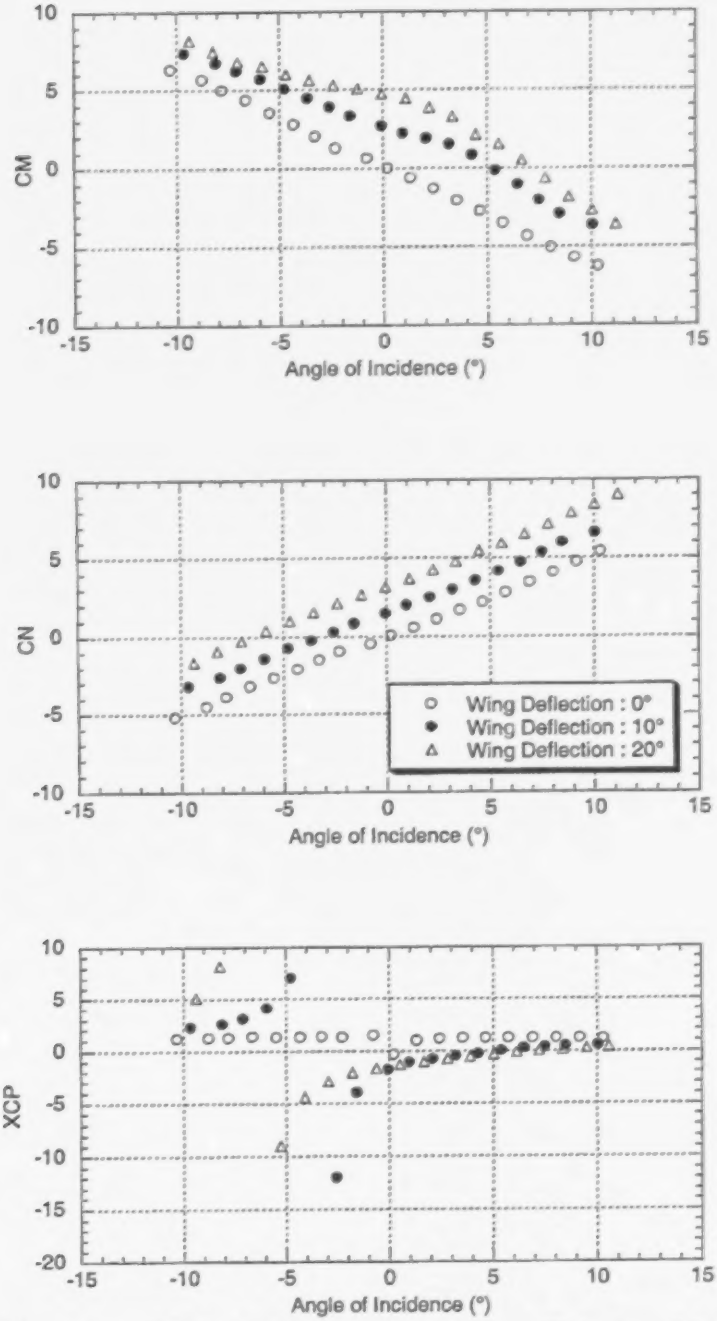

FIGURE D-16 – Configuration 4 aerodynamic coefficients at Mach 2.5
(model roll orientation : 0°)

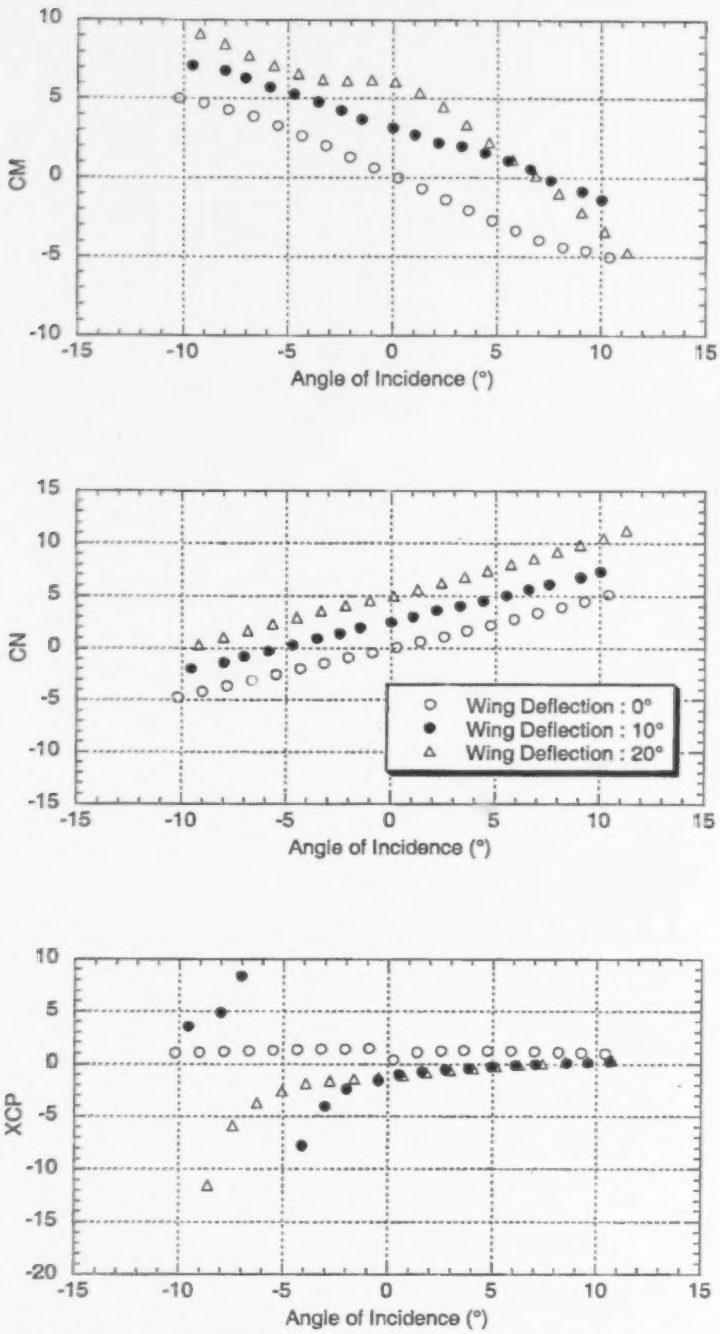

FIGURE D-17 – Configuration 4 aerodynamic coefficients at Mach 2.5 (model roll orientation : 45°)

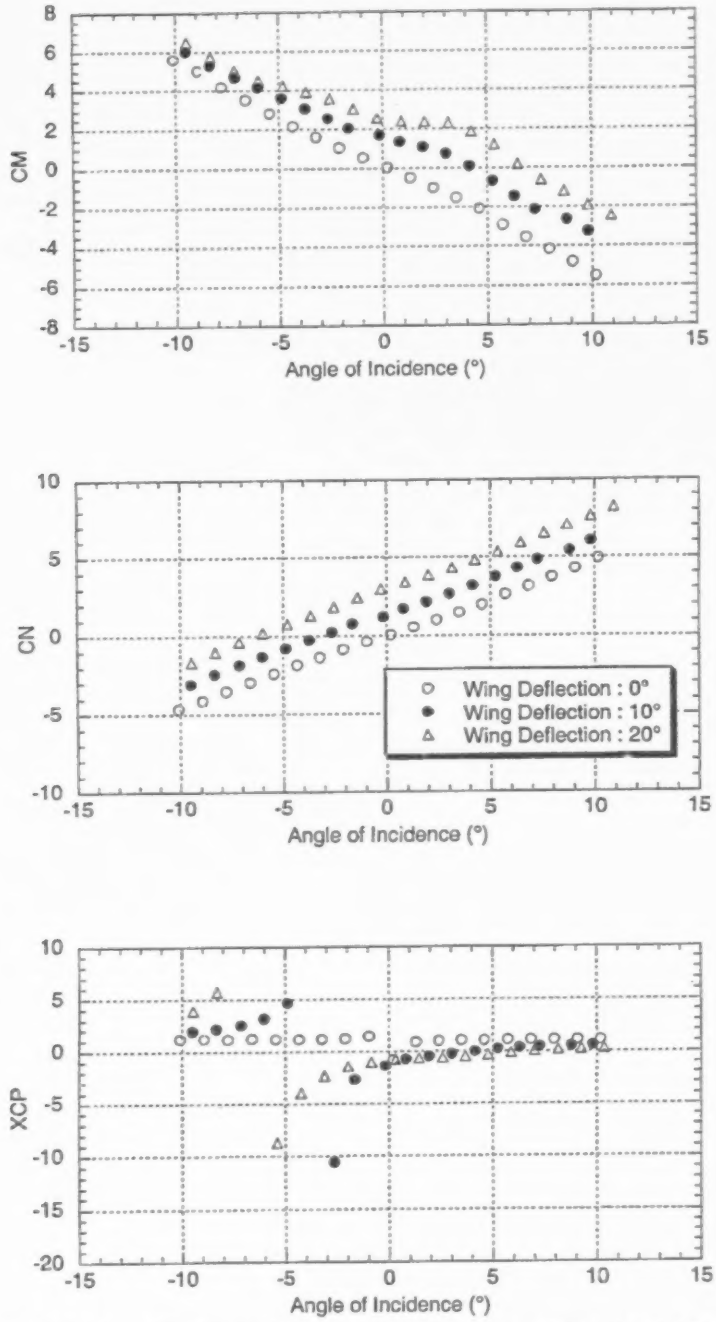

FIGURE D-18 – Configuration 4 aerodynamic coefficients at Mach 3.0 (model roll orientation : 0°)

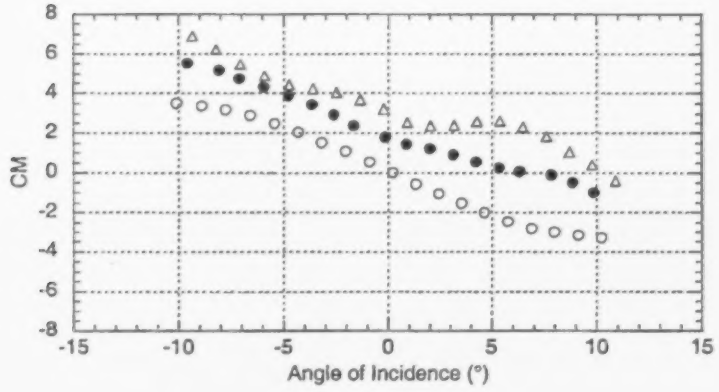

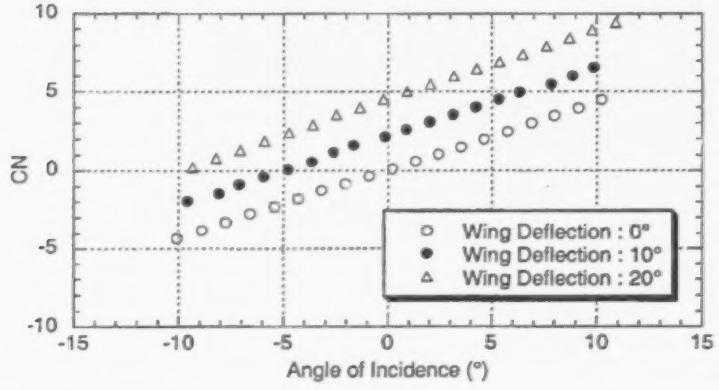

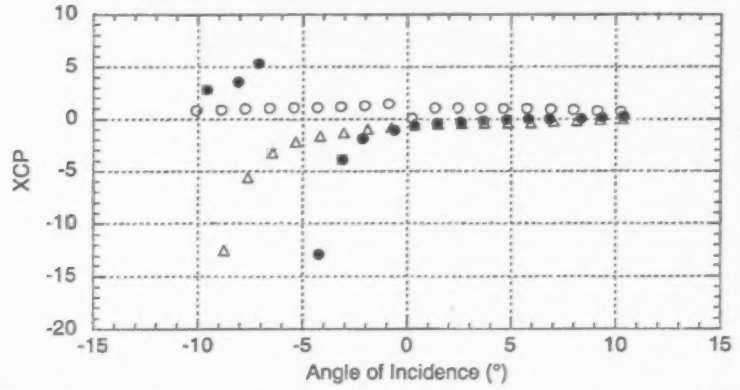

FIGURE D-19 – Configuration 4 aerodynamic coefficients at Mach 3.0
(model roll orientation : 45°)

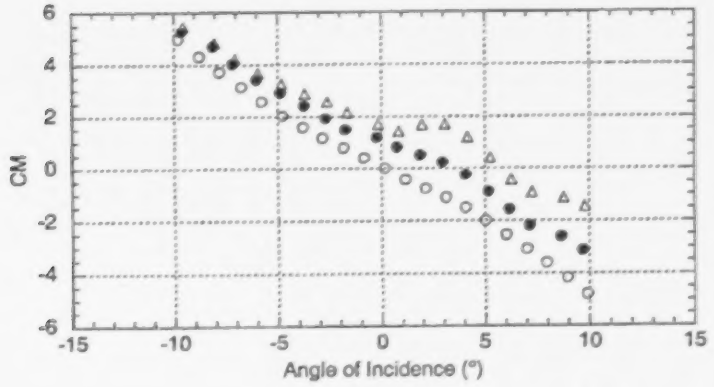

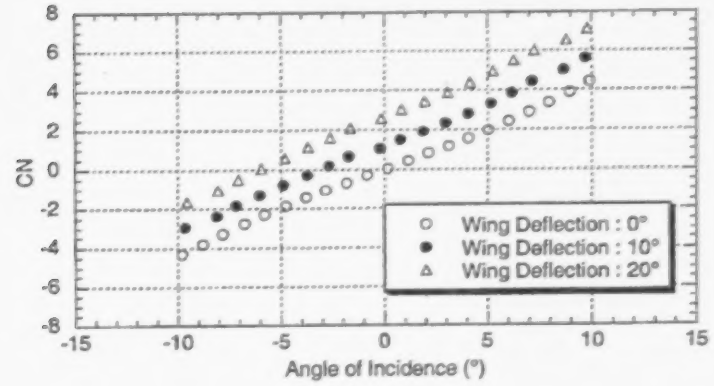

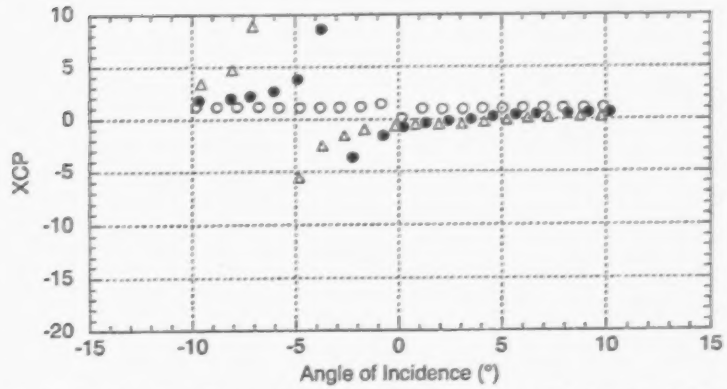

FIGURE D-20 – Configuration 4 aerodynamic coefficients at Mach 3.5
(model roll orientation : 0°)

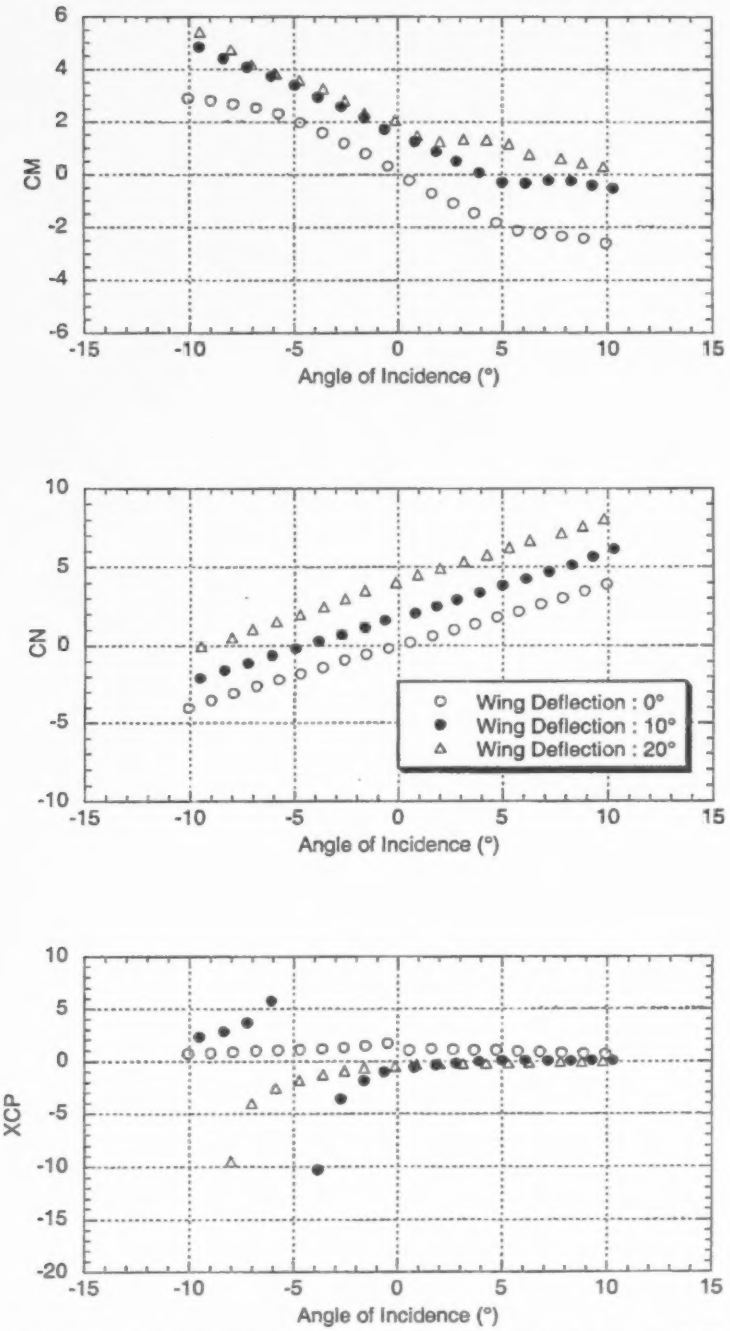

FIGURE D-21 – Configuration 4 aerodynamic coefficients at Mach 3.5
(model roll orientation : 45°)

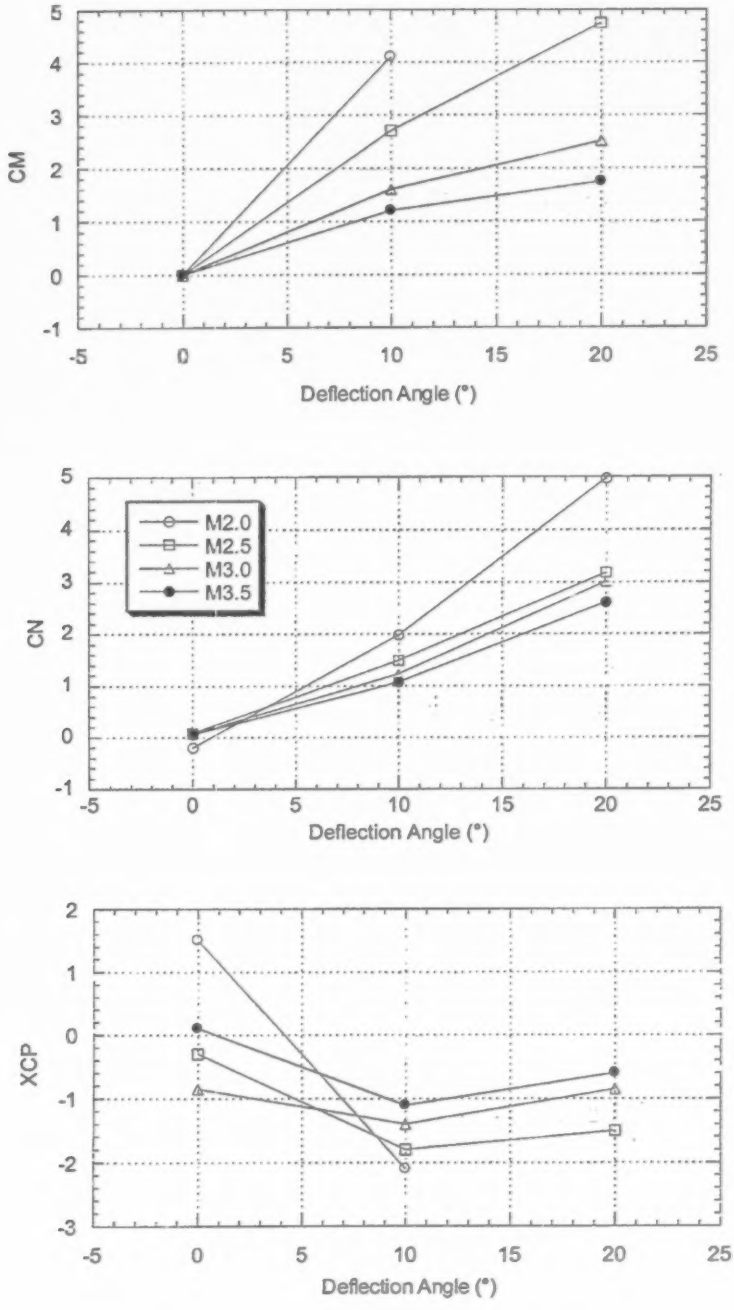

FIGURE D-22 – Configuration 4 aerodynamic coefficients for wing deflection at 0° incidence (model roll orientation: 0°)

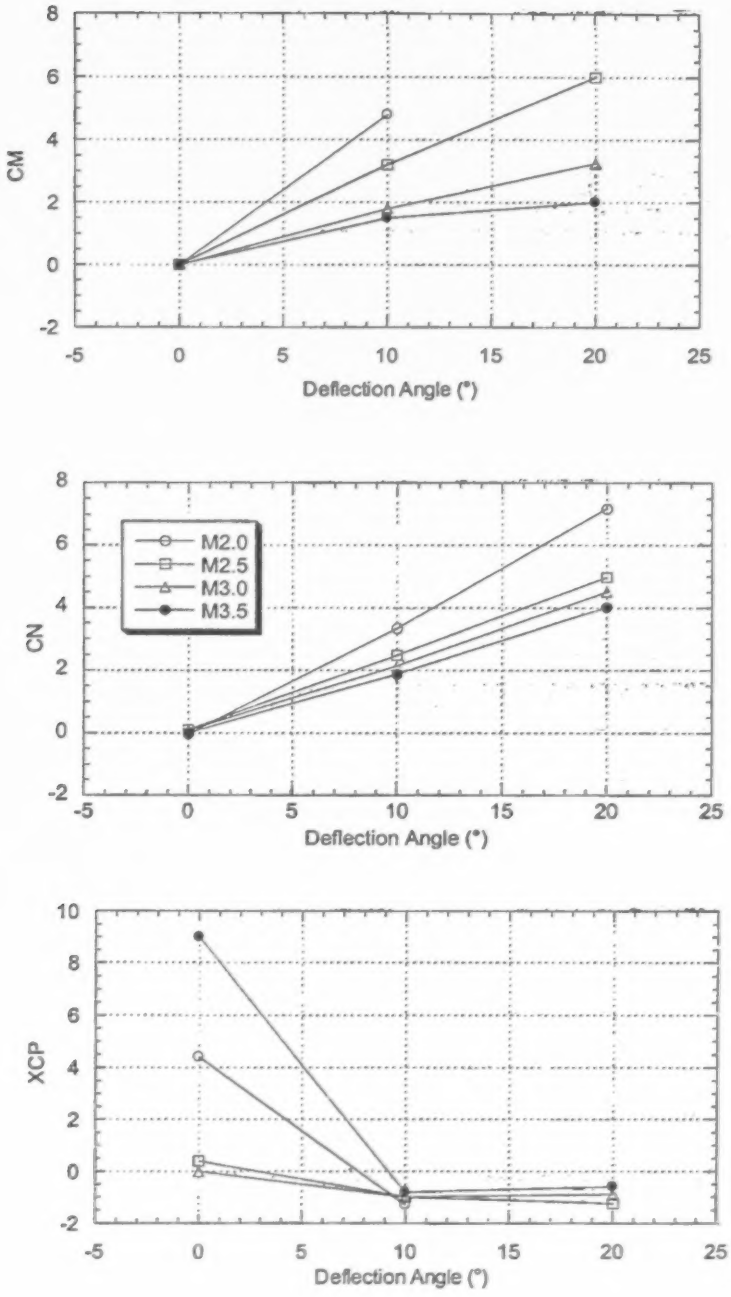

FIGURE D-23 – Configuration 4 aerodynamic coefficients for wing deflection at 0° incidence (model roll orientation: 45°)

INTERNAL DISTRIBUTION

DREV-TM-1999-050

1 - Deputy Director General
1 - Chief Scientist
1 - H/Delivery Systems Section
6 - Document Library
1 - E. Fournier (author)
1 - F. Lesage
1 - A. Dupuis
1 - B. Girard
1 - M. Lauzon
1 - P. Harris
1 – A. Jeffrey
1 – R. Bilodeau

DOCUMENT CONTROL DATA

1. ORIGINATOR (name and address)	2. SECURITY CLASSIFICATION (including special warning terms if applicable)
DREV	UNCLASSIFIED

3. TITLE (Its classification should be indicated by the appropriate abbreviation (S, C, R or U)
AERODYNAMIC COEFFICIENTS MEASUREMENT ON A MODEL OF A SPARROW AIM-7M MISSILE IN THE DREV TRISONIC WIND TUNNEL (U)

4. AUTHORS (Last name, first name, middle initial. If military, show rank, e.g. Doe, Maj. John E.)
FOURNIER, ERIC, Y.

5. DATE OF PUBLICATION (month and year)	6a. NO. OF PAGES	6b. NO. OF REFERENCES
APRIL 1999	19	7

7. DESCRIPTIVE NOTES (the category of the document, e.g. technical report, technical note or memorandum. Give the inclusive dates when a speci reporting period is covered.)
MEMORANDUM

8. SPONSORING ACTIVITY (name and address)
DREV

9a. PROJECT OR GRANT NO. (Please specify whether project or grant)	9b. CONTRACT NO.
3eb12	

10a. ORIGINATOR'S DOCUMENT NUMBER	10b. OTHER DOCUMENT NOS
DREV-TM-	N/A

11. DOCUMENT AVAILABILITY (any limitations on further dissemination of the document, other than those imposed by security classification)

- ☒ Unlimited distribution
- ☐ Contractors in approved countries (specify)
- ☐ Canadian contractors (with need-to-know)
- ☐ Government (with need-to-know)
- ☐ Defense departments
- ☐ Other (please specify)

12. DOCUMENT ANNOUNCEMENT (any limitation to the bibliographic announcement of this document. This will normally correspond to the Docum Availability (11). However, where further distribution (beyond the audience specified in 11) is possible, a wider announcement audience may selected.)
UNLIMITED ANNOUNCEMENT

13. ABSTRACT (a brief and factual summary of the document. It may also appear elsewhere in the body of the document itself. It is highly desirable that the abstract of classified documents be unclassified. Each paragraph of the abstract shall begin with an indication of the security classification of the information in the paragraph (unless the document itself is unclassified) represented as (S), (C), (R), or (U). It is not necessary to include here abstracts in both official languages unless the text is bilingual).

The present wind tunnel investigation is part of a project studying the effectiveness of reaction jet controls on missiles and projectiles. As a comparison basis between reaction jets and conventional control appendages was required, a complete database of aerodynamic coefficients had to be developed on a generic model shape. However, instead a using a generic model, it was decided to use a model of the Sparrow AIM-7M medium range missile in an effort to demonstrate the capability of DREV's wind tunnel in the experimental investigation of actual missiles, and also due to the large aerodynamic database existing on this vehicle. Testing covered a large range of Mach numbers, from 1.5 to 4.0, and angles of incidence from -10° to + 10°. Two different roll orientations of the model were studied (0° and 45°). Additionally, data involving wing deflections were also generated for the same Mach number range, over the same model incidence range, for deflection angles up to 20°. A build-up component method was used during the testing phase: data for a clean body (F1), for a body with tail fins only (F3), for a body with control wings only (F2), for a body with both sets of appendages (F4), and finally, for a body with both sets of appendages and antennas and attachment pins (F5) were generated. The database for the reaction jet project was generated and comparative results have indicated that DREV's wind tunnel can generate good technical results for missile shaped models.

14. KEYWORDS, DESCRIPTORS or IDENTIFIERS (technically meaningful terms or short phrases that characterize a document and could be helpful in cataloguing the document. They should be selected so that no security classification is required. Identifiers, such as equipment model designation, trade name, military project code name, geographic location may also be included. If possible keywords should be selected from a published thesaurus, e.g. Thesaurus of Engineering and Scientific Terms (TEST) and that thesaurus-identified. If it is not possible to select indexing terms which are Unclassified, the classification of each should be indicated as with the title.)

MISSILES, SPARROW AIM 7M, AERODYNAMIC COEFFICIENTS, FORCES

#511174